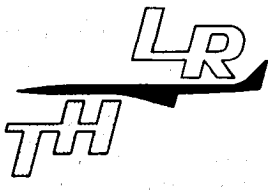

DELFT UNIVERSITY OF TECHNOLOGY

DEPARTMENT OF AEROSPACE ENGINEERING

Memorandum M-255

ESTIMATION OF DRAG AND THRUST OF JET-PROPELLED AIRCRAFT BY NON-STEADY FLIGHT TEST MANOEUVRES

by

J. A. Mulder
J. M. van Sliedregt

DELFT - THE NETHERLANDS

December 1976

ESTIMATION OF DRAG AND THRUST OF JET-PROPELLED AIRCRAFT BY NON-STEADY FLIGHT TEST MANOEUVRES

by

J.A. Mulder

J.M. van Sliedregt

Department of Aerospace Engineering
Delft University of Technology
Delft
The Netherlands

SUMMARY

When measuring aircraft performance or lift-drag characteristics in steady or non-steady flight numerical apriori information is required from engine (altitude) test facilities for an accurate determination of engine thrust. It is shown in the paper that this need for apriori information may be eliminated by an inflight calibration of the measuring probes for engines gross thrust and mass flow simultaneously with the measurement of the aircraft lift-drag characteristics.
Results are presented of 9 non-steady flight test manoeuvres with a Hawker Hunter mk VII jet aircraft at 10.000, 20.000 and 30.000 ft nominal flight altitude. Besides lift-drag characteristics and engine gross thrust and mass flow calibration factors several alternative performance characteristics as excess thrust in horizontal flight and also stability and control characteristics may be deduced from the measurements. The validity of the flight test results, in particular with respect to the inflight calibration of the gross thrust and mass flow measuring probes is, because of te particular aircraft exploited for the flight tests, restricted to the case of a socalled straight jet engine configuration and a non-flexible aircraft.

1. INTRODUCTION

Aircraft lift and drag characteristics can be measured in flight by subtracting the components of engine net thrust along and perpendicular to airspeed from the corresponding components of the total aerodynamic force.

In steady-flight conditions the components of the total aerodynamic force follow directly from the condition of steady straight flight when only the flight path angle is known. Measurements in steady-straight conditions however are time consuming and furthermore the resulting accuracies limited due to unavoidable deviations from the nominal steady-straight flight condition.

For the measurement of the components of the total aerodynamic force in non-steady flight conditions additional instrumentation is required in the form of accelerometers. Furthermore the angle of attack must accurately be known. Usually the angle of attack is measured by means of a vane positioned on a boom some distance ahead of the aircraft in order to minimize aircraft induced position errors. Still an inflight calibration in a series of steady-straight measuring runs is necessary. The question then remains to what extent this calibration applies to the non-steady flight conditions for the measurement of lift and drag.

An alternative constitutes the technique of calculating rather than measuring the angle of attack. The reliability of this technique has by now been proven in the course of several flight test programs, Ref. 7, 13 and 18.

In order to obtain accurate lift-drag data engine net thrust must accurately be known in flight. In the case of jet propulsion net thrust is indirectly derived from gross thrust and mass flow. Gross thrust and mass flow can in principle be measured by means of total pressure and temperature probes positioned in the jet pipe exit. For reliable results these measuring probes must be calibrated on an engine (altitude) test facility. The result is usually expressed in terms of gross thrust and mass flow calibration factors. The implication is that for the measurement of aircraft lift and drag characteristics numerical apriori information is required from tests on an engine (altitude) test facility.

In the present flight test technique the need for numerical apriori information is eliminated by performing an inflight rather than a static calibration of the measuring probes simultaneously with the estimation of lift and drag characteristics.

The main features of the flight test method may be summarized as:
1) inflight calibration of the gross thrust and mass flow measuring probes;
2) calculation rather than the measurement of the angle of attack;
3) measurements are made in non-steady flight;
4) besides lift and drag characteristics the calculation of several important performance and stability and control characteristics;
5) application of accurate instrumentation techniques.

Many aspects of the flight test technique have been develloped earlier, e.g. Ref. 7, where results are reported of a flight test program with a low speed piston engined aircraft.

In the present paper preliminary results are presented of a flight test program with a high subsonic jet aircraft, Fig. 1. Some data on the aircraft are given in Table 1.

Because of the particular aircraft exploited in the flight test program the validity of the results, in particular with respect to the inflight calibration of the gross thrust and mass flow measuring probes is restricted to the case of a socalled straight jet configuration and a non-flexible aircraft.

The paper has been organized as follows. In Section 3 the principles underlying the technique of calculating the angle of attack in non-steady flight are described. Section 4 provides an introduction to the

measurement of gross thrust and mass flow in flight. Furthermore the aerodynamic model and the engine model are presented. In Section 5 preliminary experimental results are described of 9 non-steady flight test manoeuvres at different nominal flight altitudes. From the 9 flight test manoeuvres 3 independent estimates of the gross thrust calibration factor could be obtained which were within 0.5% of the corresponding value of a static calibration. Concluding remarks are made in Section 6. In the appendix a brief introduction to regression analysis is presented.

2. NOTATION

A	aspect ratio, specific force (quantity sensed by an accelerometer)
A_e	exhaust area
A_e^*	effective exhaust area
a	scalar or vector of parameters
C	dimensionless coefficient, rate of climb
C_{D_o}	minimum drag coefficient
C_{L_1}	lift coefficient at minimum drag
C_{L_o}	lift coefficient at zero angle of attack
D	aircraft drag
E	expectation operator
e	Oswald factor, residual of a regression analysis
g	acceleration due to gravity
h	nominal flight altitude
i_p	angle between gross and thrust and X-axis
K_e	externally acting propulsive force
K_i	internally acting propulsive force
k_o, k_1	constants in the expression of critical Mach number
L	aircraft lift
M	flight Mach number, aerodynamic moment about Y-axis
M_c	critical Mach number
m	aircraft mass
N	number of measurements
n	engine rpm, normal load factor
n^*	"dimensionless" engine rpm $n/\sqrt{\theta}$
npr	nozzle pressure ratio p_{t_e}/p_∞
p	static pressure
p_t	total pressure
Q	mass flow
Q^*	"dimensionless" mass flow $Q\sqrt{\theta}/\delta$
q	rate of pitch
R	total aerodynamic force
R^*	resultant of lift and drag
Re	Reynolds number
R_t	total correlation coefficient
r	angular speed about Z-axis
S	wing surface area
T	thrust, static temperature
T^*	"dimensionless" thrust T/δ
T_o	static temperature at sea level S.A.
T_t	total temperature
V	airspeed, variance matrix
W	aircraft weight
w	speed of exhaust gases
X, X_w	aerodynamic force along X, resp. X_w-axis
$\mathbf{X}$	vector or matrix of independent variables
x	state vector, element of $\mathbf{X}$
x_{cg}	location of aircraft centre of gravity
x_{mp}	location of manoeuvre point
x_{np}	location of neutral point

Y	scalar or vector of dependent variable
y	element of Y
Z, Z_w	aerodynamic force along Z, resp. Z_w-axis
Δz_T	change of altitude
α	angle of attack
γ	flight path angle, ratio of specific heats
ε	equation error
δ	ratio p/p (sea level standard atmosphere)
δ_e	elevator angle
ϕ	roll angle
θ	pitch angle, ratio T_t/T_o
ρ	air density, simple correlation coefficient
σ	standard deviation

Superscript

$\dot{}$	time derivative
$\hat{}$	estimated quantity
$\bar{}$	mean quantity
T	vector or matrix transpose
-1	matrix inverse

Subscript

e	jet pipe exit
GT	gross thrust
i	engine inlet
m	measured quantity
MF	mass flow
N	net thrust
pre	pre-entry
post	post-exit
O, ∞	undisturbed air flow at infinity
x, z x_w, z_w x_T, z_T	refering to the resp. reference frames

Reference frames

All reference frames are vehicle carried, rectangular and right handed with the origin in the aircraft centre of gravity, Fig. 2.

X, Y, Z	body fixed reference frame, X, Z in the aircraft's plane of symmetry
X_w, Y_w, Z_w	air-trajectory reference frame
X_T, Y_T, Z_T	vertical reference

3. CALCULATION OF FLIGHT PATH AND ANGLE OF ATTACK IN NON-STEADY FLIGHT

As stated in Section 1 the calculation of the aircraft trajectory and in particular of the time history of the angle of attack in non-steady flight constitutes an essential aspect of the present flight test technique.

The underlying principles are briefly described in this Section. The following set of differential equations represent the kinematical relations of an aircraft in symmetrical flight in a with respect to a flat earth horizontally and uniformly moving airmass:

$$\begin{aligned} \dot{V}_{x_T} &= A_x \cos\theta + A_z \sin\theta \\ \dot{V}_{z_T} &= -A_x \cos\theta + A_z \cos\theta + g \\ \dot{\Delta z}_T &= V_{z_T} \\ \dot{\theta} &= q \end{aligned} \qquad (3\text{-}1)$$

In the present flight test technique high accuracy instrumentation techniques result in very accurate measurements of the independent variables in (3-1) i.e. A_x, A_z and q.

This means that an estimate of the time history of the state vector $\hat{x} \triangleq \text{col}\,[\hat{V}_{x_T}, \hat{V}_{z_T}, \Delta\hat{z}_T, \hat{\theta}]$ could be calculated by numerical integration of (3-1) if the initial value of x at the start of the flight test manoeuvre were exactly known.

Then also the time history of airspeed and angle of attack would follow immediately:

$$\hat{V} = \left\{ \hat{V}_{x_T}^2 + \hat{V}_{z_T}^2 \right\}^{\frac{1}{2}}$$
$$\hat{\alpha} = \hat{\theta} - \hat{\gamma}, \quad \hat{\gamma} = - \operatorname{arctg} \frac{\hat{V}_{z_T}}{\hat{V}_{x_T}} \qquad (3\text{-}2)$$

In practice the initial value of x is not exactly known.

It can be shown however that the initial value of x may be very accurately obtained by selecting that value which results in the smallest deviations between V_m and $\hat{V}$, Δz_{T_m} and $\Delta\hat{z}_T$ where V_m and z_{T_m} are directly measured with barometric transducers. This has been illustrated in Fig. 3 where different time histories result, when starting the numerical integration from different initial values.
When the initial value of x is accurately known it may be expected that the corresponding time history of α will also be very accurate.

The technique described above of calculating the time history of the angle of attack by selecting the "best" initial value of x has been succesfully applied in different flight test programs as reported in Ref. 7 and 18.

In Ref. 11 a more advanced method for the calculation of the time history of α is introduced. Two methods were compared in Ref. 13 yielding almost identical results.

4. THE ESTIMATION OF LIFT-DRAG CHARACTERISTICS AND INFLIGHT CALIBRATION OF GROSS THRUST AND MASS FLOW MEASURING PROBES

In symmetrical flight conditions the total aerodynamic force R is in the plane of symmetry of the aircraft. Per definition R is the resultant of engine net thrust T_N and the resultant of lift and drag, R^*, Fig. 4.

The components of R along and perpendicular to the airspeed vector V can be written as, e.g. Ref. 14:

$$X_w = T_{GT} \cos(\alpha + i_p) - QV - D$$
$$Z_w = - T_{GT} \sin(\alpha + i_p) - L \qquad (4\text{-}1)$$

in which QV represents engine ram drag.

X_w and Z_w can be determined in flight from the specific forces A_x, A_z and the angle of attack α according to:

$$X_w = m\,(A_x \cos\alpha + A_z \sin\alpha)$$
$$Z_w = m\,(-A_x \sin\alpha + A_z \cos\alpha) \qquad (4\text{-}2)$$

The specific forces A_x and A_z are measured with accelerometers while the angle of attack α may be calculated by applying the flight path reconstruction technique as described in Section 3.

When gross thrust T_{GT} and mass flow Q can sufficiently accurate be measured in flight, lift and drag follows directly from:

$$D = T_{GT} \cos(\alpha + i_p) - QV - X_w$$
$$L = - T_{GT} \sin(\alpha + i_p) - Z_w \qquad (4\text{-}3)$$

(4-3) is used in classical techniques for the measurement of lift and drag characteristics in steady and non-steady flight. In steady flight X_w and Z_w may be readily obtained from the flight path angle and the condition of steady flight while in non-steady flight accelerometers and an estimate of the angle of attack must be used, e.g. Ref. 10 and 14.

Gross thrust and mass flow may be determined in flight from total pressure and temperature measurements in the jet pipe exit. This however requires the calibration of the total pressure and temperature measuring equipment on an engine (altitude) test facility. The result of such a calibration is usually expressed in terms of gross thrust and mass flow calibration factors as described in Section 4.1.

In the present flight test method it is propesed to derive these calibration factors from measurements in flight simultaneously with aircraft drag. The method is based upon an aerodynamic model, which is described in Section 4.2.

4.1. THE MEASUREMENT OF GROSS THRUST AND MASS FLOW

Engine gross thrust can be defined in terms of net thrust and ram drag according to:

$$T_{GT} = T_N + QV \tag{4-4}$$

Engine net thrust is defined in Fig. 6 for the case of a straight jet configuration and idealized one dimensional flow. In Fig. 6 X_{pre} denotes the pre-entry thrust i.e. the thrust resulting from the compression of the airflow before entering the air intake, K_i is called the internal thrust and X_{post} denotes the post-exit thrust i.e. the thrust resulting from the expansion of the exhaust gases to the static pressure of the undisturbed external airflow.

Net thrust may now be written as, Ref. 2 and 19:

$$T_N = X_{pre} + K_i + X_{post} \tag{4-5}$$

In the ideal case aerodynamic mechanism's convert the pre-entry and post-exit propulsive forces into K_e acting on the outside of the engine nacelle:

$$K_e = X_{pre} + X_{post} \tag{4-6}$$

With (4-5) this results in the socalled Jones net thrust:

$$T_N = K_i + K_e \tag{4-7}$$

X_{post} can be converted into a propulsive force acting on the outside of the engine nacelle only when the exhaust gases expand isentropically to the static pressure of the undisturbed external flow. In the one-dimensional flow model post-exit expansion will occur at supersonic speeds. In practice this implies adiabatic rather than isentropic expansion and X_{post} reaches only a fraction of its theoretical value. In the socalled Pearson or Standard definition of net thrust the propulsive effect of the post-exit expansion is neglected all together resulting in a slightly less optimistic estimate of net thrust.

The two definitions of net thrust of Jones and Pearson have been compared in Fig. 7.

Because of the more realistic assumption concerning the post-exit expansion of the exhaust gases and furthermore the relatively minor differences up to moderate nozzle pressure ratio's the Pearson net thrust has been selected as the most appropriate in the present case.

Pearson gross thrust and engine mass flow can be calculated from total pressure and temperature measurements according to the following well-known formula's:

$$T_{GT} = A_e\, p_{t_e} \left\{ (\gamma + 1)\left(\frac{2}{\gamma + 1}\right) \exp\left(\frac{\gamma}{\gamma - 1}\right) - \frac{1}{npr} \right\}$$

$$Q = \frac{A_e\, p_{t_e}}{T_{t_e}} \left\{ \frac{\gamma}{R} \left(\frac{2}{\gamma + 1}\right) \exp\left(\frac{\gamma + 1}{\gamma - 1}\right) \right\}^{\frac{1}{2}} \tag{4-8}*$$

which hold for supercritical nozzle pressure ratio's (i.e. npr > 1.85) and when the mass flow entering the engine equals the mass flow leaving the jet pipe exit.

Fig. 5 presents a view of the quipment for the measurement of total pressure and total temperature in the jet pipe as exploited in the present flight test program.

In (4-8) A_e denotes the geometrical jet pipe exhaust area. When applying these relations in practive, a so called effective exhaust area A_e^* must be substituted instead. The effective exhaust area is smaller compared to the geometrical exhaust area due to the following deviations from the idealized one dimensional model of jet flow, Ref. 17.

1) In Fig. 9 a more realistic two dimensional model is presented of jet exhaust flow, e.g. Ref. 4. In the one dimensional case static pressure would have a constant value of p_e (1). Because $p_e(r) > p_e(1)$ there will be a subsonic post-exit expansion resulting in an effective exhaust area, Fig. 8.

* In the sequence T_{GT} and Q indicate gross thrust and mass flow as calculated according (4-8) in contrast to (4-1) and (4-3) were these symbols indicated actual gross thrust and mass flow.

$$A_e^* = \iint_{\substack{\text{surface of}\\ \text{sonic flow}}} \cos\phi \cdot dA < A_e \qquad (4\text{-}9)$$

Gross thrust and mass flow calculated according to (4-8) must be multiplied by the ratio A_e^*/A_e to correct for this effect of subsonic post-exit expansion. A_e^*/A_e may be interpreted as a gross thrust and mass flow calibration factor:

$$C_{GT} = C_{MF} = \frac{A_e^*}{A_e} \qquad (4\text{-}10)$$

In fig. 10 $\frac{A_e^*}{A_e}$ has been calculated for different values of nozzle pressure ratio and the parameter $\frac{\Delta p_e(o)}{p_{t_e}}$.

2) In practive a boundary layer will develope in the jet pipe which will affect gross thrust as well as mass flow. This may also be expressed in terms of a further reduction of effective exhaust area as well as in terms of a decrease of gross thrust and mass flow calibration factors.

The elliptical distribution of static pressure p_e results in identical gross thrust and mass flow calibration factors. Actual gross thrust and mass flow calibration factors may not be expected to be equal due to a different effect of the boundary layer on gross thrust and mass flow.

Prior to the present flight test program the gross thrust calibration factor was determined as a function of npr by comparing actually produced thrust T_{GT_m} with the corresponding value resulting from (4-8) during a static test of the complete aircraft:

$$C_{GT} = \frac{T_{GT_m}}{T_{GT}} \qquad (4\text{-}11)$$

resulting in the measured curve of Fig. 11.
The calculated curve is made with the help of Fig. 10 and shows the effect of the subsonic post-exit expansion. The difference between these curves, representing the effect of the boundary layer, reaches a constant value of approximately 0.03 as the npr increases. At the supercritical npr's of the flight test manoeuvres the parameter $\Delta p_e(o)/p_{t_e}$ proved to be almost constant resulting in a constant calibration factor of 0.99 for the effect of subsonic post-exit expansion as shown in Fig. 10. It may thus be concluded that in flight the gross thrust calibration factor will have an approximately constant value of 0.96.
The mass flow calibration factor cannot be determined without an engine (altitude) test facility. From Fig. 10 it follows that the mass flow calibration factor will be smaller than 0.99 because of the effect of the boundary layer. Experience from altitude test facilities has shown that, in contrast to the gross thrust calibration factor, the mass flow calibration factor may vary as a function of flight altitude, e.g. Ref. 3.

4.2. THE AERODYNAMIC AND ENGINE MODEL

A polar drag curve may be postulated according to:

$$C_D = C_{D_o} + \frac{(C_L - C_{L_1})^2}{\pi Ae} \qquad (4\text{-}12)$$

Substitution of (4-12) into (4-1) results in:

$$X_w = C_{GT}\, T_{GT} \cos(\alpha + i_p) - C_{MF}(h)\, QV - \left(C_{D_o} + \frac{(C_L - C_{L_1})^2}{\pi Ae}\right) \tfrac{1}{2}\rho V^2 S$$

This may be written in dimensionless form with $i_p = 0$:

$$C_{X_w} = C_{X_{W_o}} + C_{GT}\frac{T_{GT}}{\tfrac{1}{2}\rho V^2 S}\cos\alpha - C_{MF}(h)\frac{QV}{\tfrac{1}{2}\rho V^2 S} + \\ + C_{X_{wC_L}}\, C_L + C_{X_{wC_L^2}}\, C_L^2 \qquad (4\text{-}13)$$

In (4-13) the lift coefficient C_L may be obtained from (4-1) in dimensionless from:

$$C_L = - C_{Z_w} - C_{GT}\frac{T_{GT}}{\tfrac{1}{2}\rho V^2 S} \cdot \sin(\alpha + i_p) \approx - C_{Z_w} - \frac{T_{GT}}{\tfrac{1}{2}\rho V^2 S}\sin\alpha \qquad (4\text{-}14)$$

because $\frac{T_{GT}}{\frac{1}{2}\rho V^2 S} \sin\alpha$ is small compared to C_{Z_w}.
No supercritical drag rise is modeled, therefore (4-13) applies only to the subcritical flight region. The subcritical flight region is defined by:

$$M < M_c \quad \text{with} \quad M_c = \frac{1}{k_o + k_1 |C_L|} \tag{4-15}$$

Approximate values of the constants in (4-15) for the present case follow from Ref. 8; $k_o = 1.2$, $k = 0.4$. The resulting critical Mach number is presented in Fig. 12.

The lift coefficient C_L may be written as:

$$C_L = C_{L_o} + C_{L_\alpha}(M) \ (\alpha - \alpha_o)$$

A quadratic model is postulated for the variation of C_{L_α} as a function of Mach number:

$$C_{L_\alpha} = C_{L_\alpha} + C_{L_{\alpha M}} M + C_{L_{\alpha M^2}} M^2$$

resulting in the following expression for C_L:

$$C_L = C_{L_o} + C_{L_\alpha} \alpha_o + C_{L_{\alpha M}} \alpha_o M + C_{L_{\alpha M^2}} \alpha_o M^2 + C_{L_\alpha} \cdot \alpha + C_{L_{\alpha M}} \alpha M$$

$$+ C_{L_{\alpha M^2}} \alpha M^2 \approx$$

$$C_{L_o} + C_{L_\alpha} \alpha + C_{L_{\alpha M}} M + C_{L_{\alpha M^2}} M^2 \tag{4-16}$$

because α_o is very small.
(4-13) and (4-16) represent approximate models of dimensionless excess thrust C_{X_w} and lift coefficient C_L. Additional terms might be added to account for the effects of Reynolds number variations, elevator angle, non-steadiness of the airflow etc. The significance of these additional terms may be examined when analyzingactual flight test data. In the present case the effect of adding one or more of these terms to the models of excess thrust and lift coefficient proved to be very small.
The pitch moment coefficient is written in the usual form:

$$C_m = C_{m_o} + C_{m_\alpha} \cdot \alpha + C_{m_q} \cdot \frac{q\bar{c}}{V} + C_{m_\delta} \cdot \delta_e \tag{4-17}$$

in which the derivatives C_{m_o}, C_{m_α}, C_{m_q} and C_{m_δ} for a given location of the aircraft centre of gravity may be expected to vary as a function of Mach number.

The aerodynamic model of the pitch moment does play a role in the correction methods described in Section 5.2. in particular with respect to the calculation of various stability and control characteristics. Most of these results will be left to a future report.

From Ref. 1 it follows finally that dimensionless gross thrust T_{GT}^* and mass flow Q^* may be written as a function of two dimensionless parameters n^* and M:

$$T_{GT}^* = T_{GT}^* \ (n^*, M)$$

$$Q^* = Q^* \ (n^*, M) \tag{4-18}$$

In (4-18) the effect of viscosity has been neglected. Furthermore these relations do hold only when the compressor inlet guide vanes are fixed in one position. In the present series of flight test measurements these guide vanes have always been in the fully open position.

The engine model (4-18) may be identified simultaneously with the parameters in the aerodynamic model of C_{X_w}, C_L and C_m. The resulting models are used in the above mentioned correction methods for the calculation of various performance and stability and control characteristics as described in Section 5.2.

5. EXPERIMENTAL RESULTS

The flight test program consisted out of 19 flight during which 45 non-steady flight test manoeuvres were executed and recorded. All measurements were made in nominally symmetrical flight conditions. In this Section the results are presented of 9 manoeuvres at three different nominal flight altitudes of 10.000, 20.000 and 30.000 ft.

For a proper interpretation of the results the shape of the non-steady flight test manoeuvre must first be described. Each manoeuvre is commenced at low speed and approximately steady symmetrical horizontal flight. The engine thrust is increased to a preselected level resulting in a longitudinal acceleration at nominally constant flight altitude.
Because the normal load factor remains close to 1 and rate of pitch (or aerodynamic pitch moment) small this would result in a quasi-steady increase of airspeed until a steady horizontal flight condition is reached. However at various instants regulary spaced in time the quasi-steady motion is interrupted and a non-steady pull-up-push-down type of manoeuvre is executed by means of the elevator control.
In Fig. 13 time histories of the specific force along the vertical axis and the flight Mach number may illustrate the verbal description of the flight test manoeuvre.

From the measurements made of the flight test manoeuvre, performance as well as stability and control characteristics may be derived. In those cases, for instance during the initial phase of a flight test program, when performance characteristics are of a major concern compared to quantitative assesment of stability and control characteristics the non-steady pull-up-push-down manoeuvres need not to be executed.

A description of the flight test instrumentation system is presented in Ref. 9. In flight 20 variables are sampled and recorded in digital form at a rate of 20 per second. The resolution of the measurement system equals 0.01%. The accuracy of the inertical transducers is of the order of 0.01%, the accuracy of the barometric transducers is of the order of 0.1%.

5.1. IDENTIFICATION OF THE AERODYNAMIC AND ENGINE MODEL

The relations (4-13), (4-16), (4-17) constitute the aerodynamic and (4-18) the engine model. These relations may all be written symbolically as:

$$y(i) = a_o\, x_o(i) + a_1\, x_1(i) + \ldots + a_r\, x_r(i) \tag{5-1}$$

in which i refers to a particular time instant t_i during the flight test manoeuvre. As described in the previous Sections $y(i)$, $x_o(i)$, $x_1(i)$, ..., $x_r(i)$ are measured in flight. The residual $e(i)$ is defined as:

$$e(i) = y(i) - \hat{a}_o\, x_o(i) - \hat{a}_1\, x_1(i) \ldots - \hat{a}_r\, x_r(i) \tag{5-2}$$

which will in general not be zero because of modelling and measurement errors. Least squares or regression estimates of the parameters in (5-1) can be calculated by minimizing $\sum_{i=1}^{N} e^2(i)$ with respect to $\hat{a}_o$, $\hat{a}_1$, ..., $\hat{a}_r$. The parameter estimation accuracies may be expressed in terms of a variance matrix which can be derived from the measurements simultaneously with the least squares estimates of the parameters.

A basic problem constitutes the selection of the "optimum" number of parameters in the model (5-1). It is shown in the Appendix that too many parameters result in unacceptably low estimation accuracies while a model which is to simple (i.e. a model in which one or more important parameters are missing) generates large equation errors or residuals.

A case in which the model did contain to many parameters has been encountered in the present flight test program with respect to the estimation of the parameters in the aerodynamic model of C_{X_w} (4-13). Because some of these parameters represent gross thrust and mass flow calibration factors as discussed in Section 4 the solution of this estimation problem is of particular importance.

It is well known that the mass flow calibration factor does vary as a function of flight altitude. Taking the mass flow calibration factor at 10.000 ft nominal flight altitude as a reference the following incremental mass flow calibration factors may be defined as:

$$\Delta C_{MF}(20) = C_{MF}(10) - C_{MF}(20)$$

$$\Delta C_{MF}(30) = C_{MF}(10) - C_{MF}(30)$$

in which the numbers 10, 20 and 30 refer to the nominal flight test manoeuvre altitudes of 10.000, 20.000 and 30.000 ft.

(4-13) may now be written as:

$$\begin{aligned} C_{X_w} = C_{X_{w_o}} &+ C_{GT}\,\frac{T_{GT}}{\tfrac{1}{2}\rho V^2 S}\cos\alpha - C_{MF}(10)\,\frac{QV}{\tfrac{1}{2}\rho V^2 S} \\ &+ \Delta C_{MF}(20)\,\frac{Q(20)\,V}{\tfrac{1}{2}\rho V^2 S} + \Delta C_{MF}(30)\,\frac{Q(30)\,V}{\tfrac{1}{2}\rho V^2 S} \\ &+ C_{X_{w_{C_L}}} \cdot C_L + C_{X_{w_{C_L^2}}} \cdot C_L^2 \end{aligned} \tag{5-3}$$

In (5-3) the variable $\frac{Q(20)\,V}{\tfrac{1}{2}\rho V^2 S}$ is identical to $\frac{QV}{\tfrac{1}{2}\rho V^2 S}$ at 20.000 ft but vanishes at the other nominal flight

altitudes. The same holds for $\frac{Q(30)\ V}{\frac{1}{2}\rho V^2 S}$ with respect to 30.000 ft nominal flight altitude. In contrast to (4-13), (5-3) contains only constant parameters while valid all the same for different nominal flight altitudes. An attempt can now be made to estimate these parameters by means of a regression analysis.

Because (5-3) does hold only in the subcritical flight regime (supercritical drag rise has not been modelled) only the subcritical data points of the flight test manoeuvres must be selected for the regression analysis. Therefore for the present, supercritical data points will be neglected. The next step is to also neglect the data points in the strongly non-steady parts of the flight test manoeuvres. This still leaves an ample amount of measurements and does eliminate beforehand the problemen of aerodynamic model inaccuracies in non-steady flight conditions.

The results of a regression analysis taking the remaining data points of a flight test manoeuvre at 10.000, 20.000 and 30.000 ft nominal flight altitude together, are presented in Table 2 and 3. It follows from Table 3 that the estimation errors of the gross thrust and mass flow calibration factors and the constant part of C_{X_w} are very highly correlated. This results in very high estimation errors and does indicate the model must be simplified in order to improve the accuracy of the results.

In Table 2 and 4 the results are presented of a simplified model resulting when substotuting $C_{MF}(10) = C_{GT}$ in (5-3). It follows that the simplified model does equally well fit to the measurements while the correlation between the parameter estimation errors has considerably been reduced. This usually goes hand in hand with a significant improvement of parameter estimation accuracies as shown in Table 5. Results of 9 flight test manoeuvres are given in Fig. 14 and 15. It follows that the estimated gross thrust calibration factors are within 0.5% from the corresponding value of the static calibration discussed in Section 4. It follows from (5-3) that a parabolic polar drag curve can be calculated by substituting the estimated parameter values into:

$$C_D = - C_{X_{w_o}} - C_{X_{w_{C_L}}} \cdot C_L - C_{X_{w_{C_L^2}}} \cdot C_L^2 \qquad (5\text{-}4)$$

The results are given in Fig. 16.

Fig. 19 shows mean and $\pm$ 1σ region of 9 polar drag curves resulting when, as in the classical technique for the measurement of lift-drag characteristics, (4-3) is applied using one set of values of the gross thrust and mass flow calibration factors. The range of subcritical C_L values traversed in the quasi-steady portions of the flight test manoeuvres is approximately from 0.1 to 0.35. It follows that the corresponding maximum dispersion in terms of standard deviation of C_D amounts up to 4 to 5 drag counts. The dispersion of the individual curves however did not appear to be fully random in the statistical sense: curves from different nominal flight altitudes were mutually slightly "rotated". This effect might be ascribed to a minor, but yet unidentified aerodynamic model error.

Results of a regression analysis with the model of C_L (4-16) are given in Tabel 6 and 7. Only subcritical, quasi-steady data points were selected as described above and also three flight test manoeuvres at different nominal flight altitudes were taken together. The relatively high correlations between estimation errors of C_{L_α}, $C_{L_{\alpha M}}$ and $C_{L_{\alpha M^2}}$ and the corresponding limited estimation accuracies need not be of much concern now because the interest is usually restricted to the resulting estimate of $C_{L_\alpha}(M)$ and C_L according to:

$$C_{L_\alpha}(M) = C_{L_\alpha} + C_{L_{\alpha M}} \cdot M + C_{L_{\alpha M^2}} \cdot M^2 \qquad (5\text{-}5)$$

and:

$$C_L = C_{L_o} + C_{L_\alpha}(M)\ (\alpha - \alpha_o) \qquad (5\text{-}6)$$

in which the individual parameter estimation errors do to a certain extent cancel out. Estimates of $C_{L_\alpha}(M)$, C_{L_o} and C_L as obtained from 9 flight test manoeuvres are presented in Fig. 17, 18 and 20.

Results of the estimation of the aerodynamic moment derivatives in (4-17) will be presented in a future report. In contrast to the estimation of the parameters in the model of C_{X_w} and C_L, here data points in the non-steady parts of the flight test manoeuvres are essential for the accuracy of the resulting estimates.

Finally the results of regression analyses with the engine model are given in Table 8. In this case also the accuracy of T_g^* and Q^* calculated from (4-18) is more important than the accuracies of the individual parameters in the model.

5.2. THE CALCULATION OF VARIOUS PERFORMANCE AND STABILITY AND CONTROL CHARACTERISTICS

In Section 4 an aerodynamic model was postulated for the aerodynamic forces X_w and Z_w, the aerodynamic moment M and also an engine model for gross thrust and mass flow.

The parameters in these models can be estimated from measurements in quasi-steady or non-steady flight as described in Section 5.1. After these models have been identified they may be exploited for the calculation of various performance, stability and control characteristics.

The principle is to correct the measurements for deviations from a given set of nominal standard conditions (like c.g., W, rpm, flight altitude, T), and to a set of different symmetrical flight conditions:

1) Steady straight flight with prescribed engine rpm.
2) Steady horizontal flight.
3) Accelerating horizontal flight.
4) Horizontal manoeuvring flight (i.e. $C_m = 0$, normal load factor differs from 1).

The data points to which these corrections are applied are selected such that the magnitudes of these corrections can be expected to be relatively small.
For instance, data points during quasi-steady flight are used when correcting to flight condition 1), 2) and 3) while data points in the non-steady parts of the manoeuvre are exploited when correcting to flight condition 4).

The corrections are calculated using the aerodynamic and engine model which were identified earlier. When the corrections are small, model errors will have a neglectable effect on the results and.thus any scatter must be attributed to measurement errors, atmospheric disturbances and inexact knowledge of aircraft-weight and c.g. location. For a more detailed discussion reference can be made to Ref. 15.
Fig.'s 21 to 27 present results of correcting the data point in quasi-steady flight, while Fig.'s 28 to 32 present results of correcting data points in non-steady flight to the specific symmetrical flight conditions defined above.
In Fig.'s 21, 22, 25, 26, 28 and 29 indivial corrected data points of one flight test manoeuvre are shown while in Fig.'s 23, 24 and 25 different flight test manoeuvres have been compared. From these figures it may be deduced that aircraft performance characteristics as rate of climb in steady straight flight and excess thrust in horizontal straight as well as in horizontal manoeuvering flight could be determined accurately in quasi-steady and non-steady flight.

6. CONCLUSIONS

In the case of straight jet propulsion and a rigid aircraft it is shown that measurements of lift and drag characteristics can be made without the need for numerical apriori information in the form of gross thrust and mass flow calibration factors from tests on an engine (altitude) test facility. These calibration factors may be estimated in flight simultaneously with aircraft lift and drag. Three independent flight estimated values of the gross thrust calibration factor proved to be within 0.5% of the corresponding value of a static thrust calibration. It has further been shown that various performance and stability and control characteristics may simultaneously be obtained from the measurements.

7. REFERENCES

1. AGARD, Flight test manual, Volume 1, Performance, 1959.

2. An., "Definitions of the thrust of a jet engine and of the internal drag of a ducted body", The Journal of the Royal Aeronautical Society, Volume 59, No. 536, August 1955.

3. J.C. Ascough, "Procedures for the measurement of engine thrust in flight", AGARD Flight Mechanics Symposium on "Flight Test Techniques", Cologne, October 1976.

4. T.W. Davidson, "Measurement of net thrust in flight", Journal of Aircraft, Vol. 1, No. 3, May-June 1964.

5. H. Mc.Donald, P.F. Hughes, "High subsonic after body drag", Journal of Aircraft, Vol. 2, No. 3, June 1965.

6. N.R. Draper, H. Smith, "Applied Regression Analysis", John Wiley & Sons, Inc., March 1968.

7. O.H. Gerlach, "Determination of performance and stability parameters from non-steady flight test manoeuvres", SAE paper no. 700236, March 1970.

8. S.F. Hoerner, "Fluid-dynamic drag", 1958.

9. R.J.A.W. Hosman, "Advanced flight test instrumentation: design and calibration", AGARD Conference proceedings no. 172 on "Methods for Aircraft State and Parameter Identification", November 1974.

10. K.W. Lliff, "Maximum likelihood estimates of lift and drag characteristics obtained from dynamic aircraft maneuvers", AIAA 3rd Atmospheric Flight Mechanics Conference, Arlington, Texas, June 1976.

11. H.L. Jonkers, "Application of the Kalman filter to flight path reconstruction from flight test data including estimation of instrumental bias errors", Report VTH-162, Department of Aerospace Engineering, Delft University of Technology, February 1976.

12. H.W. Kleingeld, "Design and evaluation of a symmetric flight test manoeuvre for the estimation of performance, stability and control characteristics", AGARD Conference Proceedings no. 172 on "Methods for Aircraft State and Parameter Identification", November 1974.

13. J.A. Mulder, "Estimation of the aircraft state in non-steady flight", AGARD Conference Proceedings no. 172 on "Methods for Aircraft State and Parameter Identification", November 1974.

14. E.C. Rooney, "Development of techniques to measure in-flight drag of a U.S. Navy fighter airplane and correlation of flight measured drag with wind tunnel data", AGARD Conference Proceedings No. 124 on "Aerodynamic Drag", April 1973.

15. J.M. van Sliedregt, J.A. Mulder, "Procedures for the calculation of performance, stability and control characteristics from non-steady flight data", Memorandum M-256, Department of Aerospace Engineering, Delft University of Technology, to be published.

16. J. Stephenson, R.T. Shields, D.W. Bottle, "An investigation into the pitot rate method of measuring turbo jet engine thrust in flight", A.R.C. Technical Report, C.P. No. 143 (15, 509), 1954.

17. J.P.K. Vleghert, "Bepaling van de stuwkracht van straalmotoren", Report TM1922, National Aerospace Laboratory, March 1964.

18. R.C. Wingrove, "Applications of a technique for estimating aircraft states from recorded flight test data", AIAA paper 72-965, 1972.

19. H. Wittenberg, "The propulsion of supersonic airplanes", De Ingenieur, Vol. 74, No. 6, February 1962.

8. APPENDIX, REGRESSION ANALYSIS

For the sake of completeness a brief introduction to regression analysis is presented in this Section. For a more detailed treatment reference can be made to the literature, e.g. Ref. 6.

In regression analysis the following problem is posed. Estimate the parameters a_o, a_1, ..., a_r of the linear model:

$$y(i) = a_o\, x_o(i) + a_1\, x_1(i) + \ldots + a_r\, x_r(i) + \varepsilon(i) \qquad \text{(a-1)}$$

when N sets of values are given of the independent variables $x_o(i)$, $x_1(i)$, ..., $x_r(i)$ and the dependent variable $y(i)$, while $\varepsilon(i)$ is unknown.
In (a-1) $\varepsilon(i)$ results from model or measurement errors. $\varepsilon(i)$ is usually assumed to be adequately represented by an independent random sequence with:

$$E\{\varepsilon(i)\} = 0$$

$$E\{\varepsilon(i)\ \varepsilon(j)\} = \sigma^2\, \delta_{ij}$$

$$i = 1, \ldots, N$$

(a-1) can be written more compactly by defining the row vector $X(i) = [x_o(i), x_1(i), \ldots, x_r(i)]$ and the column vector $a = \text{col}\ [a_o, a_1, \ldots, a_r]$:

$$y(i) = X(i)\ a + \varepsilon(i)$$

$$i = 1, \ldots, N \qquad \text{(a-2)}$$

In regression analysis it will be convenient to manipulate with all N equations (a-2) simultaneously. To achieve this, the N dimensional column vectors Y and ε are defined as $Y = \text{col}\,[y(o), y(1), \ldots, y(N)]$ and $\varepsilon = \text{col}[\varepsilon(1), \varepsilon(2), \ldots, \varepsilon(N)]$. Furthermore the N x r matrix X is defined as:

$$X = \begin{bmatrix} X(1) \\ X(2) \\ \vdots \\ X(N) \end{bmatrix}$$

after which (a-2) can be written as:

$$Y = Xa + \varepsilon \qquad \text{(a-3)}$$

When $\hat{a}$ is an estimate of the parameter vector a the residual e(i) is defined as $e(i) = y(i) - X(i)\hat{a}$. Defining the N dimensional vector e in the usual way by $e = \text{col}\ [e(1), e(2), \ldots, e(N)]$ the sum of the squares of the residuals e(i) can be written as:

$$e^T e = (Y - X\hat{a})^T\ (Y - X\hat{a}) \qquad \text{(a-4)}$$

The least squares estimate of a is obtained by minimizing (a-4) with respect to $\hat{a}$. A necessary condition for $\hat{a}$ to minimize (a-4) is:

$$\frac{\partial e^T e}{\partial \hat{a}} = 0 \qquad \text{(a-5)}$$

Substitution of (a-4) in (a-5) leads directly to the socalled normal equations:

$$[X^T X]\ \hat{a} = X^T Y \qquad \text{(a-6)}$$

When the matrix $[X^TX]$ is positive definite (i.e. its inverse exists) the least squares estimate of a follows from:

$$\hat{a} = [X^TX]^{-1} X^TY \tag{a-7}$$

Besides the numerical value an important characteristic of the least squates estimate constitutes the accuracy of $\hat{a}$ which is expressed by:

$$\Delta a = \hat{a} - E(\hat{a}) \tag{a-8}$$

$E(\hat{a})$ can be calculated by substituting (a-3) into (a-7) which then yields:

$$E(\hat{a}) = E\left\{[X^TX]^{-1} X^TX\, a + [X^TX]^{-1} X^T\, \varepsilon\right\} = a \tag{a-9}$$

because $E(\varepsilon) = 0$. This means that $\hat{a}$ is a socalled inbiased estimate of a.
The variance matrix of the estimation errors Δa may now be written as:

$$V(\hat{a}) = E\left\{\Delta a\, \Delta a^T\right\} = E\left\{[\hat{a} - E(\hat{a})]\, [\hat{a} - E(\hat{a})]^T\right\} =$$
$$= E\left\{[\hat{a} - a]\, [\hat{a} - a]^T\right\} \tag{a-10}$$

Substitution of (a-7) then results in:

$$V(\hat{a}) = \sigma^2\, [X^TX]^{-1} \tag{a-11}$$

From (a-11) the matrix of simple estimation error correlation coefficients may be obtained from:

$$[\rho_{ij}] = \frac{V_{ij}}{\left\{V_{ii}\, V_{jj}\right\}^{\frac{1}{2}}}$$

In many applications σ^2 is not precisely known. This will be the case in particular when $\varepsilon(i)$ must be attributed to model errors rather than measurement errors of y(i).

Then σ^2 may be estimated by:

$$\hat{\sigma}^2 = \frac{1}{n - r - 1}\, e^Te \tag{a-12}$$

which can be calculated posterior to the calculation of $\hat{a}$.
The goodness of fit of the mathematical model to the measurements is expressed by the so called total correlation coefficient R_t defined as:

$$R_t = \left\{1 - \frac{e^Te}{y^Ty}\right\}^{\frac{1}{2}}, \qquad 0 \leq R_t \leq 1$$

In case of perfect fit $e^Te = 0$ and thus $R_t = 1$. When the model (a-3) is completely invalid the parameter estimate will be identical zero:

$$\hat{a} = 0$$

because of: $X^TY = 0$

Then it follows that $e = Y$ and R_t reaches its minimum value of zero.
(a-7), (a-11) and (a-12) are well known results in regression analysis.

In flight testing problems,when accurate instrumentation systems are exploited errors measurement errors can be relatively small. It is therefore important to further evaluate the effect of modelling errors on the accuracy and the numerical value of the least square estumate $\hat{a}$.

Assume the actual model to be:

$$Y = X_1a_1 + X_2a_2 + \varepsilon \tag{a-13}$$

in which a_1 and a_2 are r and s dimensional vectors of parameters.

A least squares estimate of a_1 is made by using a simplified model

$$Y = X_1 a_1 \tag{a-14}$$

Minimization of $e_1^T e_1$ with $e_1 = Y - X_1 \hat{a}_1$ leads via the necessary conditions to the set of normal equations:

$$[X_1^T X_1]\ \hat{a}_1 = X_1^T Y \tag{a-15}$$

and the estimate of a_1:

$$\hat{a}_1 = [X_1^T X_1]^{-1}\ X_1^T Y \tag{a-16}$$

when $[X_1^T X_1]$ is positive definite.

From:

$$E(\hat{a}_1) = [X_1^T X_1]^{-1}\ X_1^T\ E(y) = [X_1^T X_1]^{-1}\ X_1^T\ [X_1 a_1 + X_2 a_2] =$$

$$= a_1 + [X_1^T X_1]^{-1} [X_1^T X_2]\, a_2 \tag{a-17}$$

follows that now $\hat{a}_1$ will in general be a biased estimate of a_1.
The estimate variance of the residuals may now be obtained from:

$$\hat{\sigma}_1^2 = \frac{1}{N - r - 1}\, e_1^T e_1 \tag{a-18}$$

In practical applications a major problem is the selection of the "optimum" number of parameters in the mathematical model of the physical proces. In general a trade off must be made between reduced extimation accuracies after an additional parameter is added and a better fit of the model to the measurements. This may be clarified as follows.

The matrix X_2 can always be written as:

$$X_2 = X_1 C + \Delta X_2 \tag{a-19}$$

in which C denotes a constant r x s matrix. It follows from (a-19) that each column of the matrix X_2 may be constituted out of a linear combination of the colums of the matrix X_1 and one column of the matrix ΔX_2.

The following important results may now be derived.

1) When ΔX_2 is very small, i.e. the columns of X_2 depend linearly on the columns of X_1, the estimate of the parameter a_1 using the simplified model will be biased according to:

$$E(\hat{a}_1) = a_1 + C a_2$$

When attempting however to eliminate this bias by adding the parameters a_2 to the model it can be shown that:
a) $\hat{\sigma}_1^2 = \hat{\sigma}^2$, the variance of the residuals has not been decreased,
b) parameter estimation errors tend to infinity due to singularity of the matrix $X^T X$, one or more simple correlation coefficients in the estimation error correlation matrix will approach 1.

2) In case all elements of C are identical zero ($X_2 = \Delta X_2$), the estimate of the parameter a_1 using the simplified model will be unbiased because of:

$$X_1^T\, \Delta X_2 = 0$$

When adding now the parameters a_2 to the model it follows that:

a) $\hat{\sigma}_1^2$ decreases to $\hat{\sigma}^2$,
b) parameter estimation errors of a_1 will remain unchanged.

It may be deduced that in case 1) extra parameters should not, while in case 2) extra parameters may be added to the model. In practical situations the decision whether or not to add an extra parameter to the model might be more difficult to make.

Length	14.90 m
Wing span	10.26 m
Wing surface	33.30 m^2
¼ chord wing sweep angle	40°
Max. take of weight	9752 kgf
Engine type	Rolls Royce Avon 122
Max. thrust at sea level	3450 kgf

Table 1. Some data on the Hawker Hunter mk VII laboratory aircraft.

	flight altitude (ft)	Model 1	Model 2
$\bar{e}$ (drag counts	10.000 20.000 30.000	+0.12 -0.01 -0.09	+0.12 -0.02 -0.09
σ_e (drag counts	10.000 20.000 30.000	4.29 3.52 2.08	4.15 3.63 2.13
$\dot{R}_t$		0.999398	0.999402

Model 1. Three thrust calibration parameters: $C_{MF}(10) = C_{GT}$, $\Delta C_{MF}(20)$, $\Delta C_{MF}(30)$.

Model 2. Four thrust calibration parameters: C_{GT}, $C_{MF}(10)$, $\Delta C_{MF}(20)$, $\Delta C_{MF}(30)$.

Table 2. Total correlation coefficients and residuals of regression analysis with different models of C_{X_w}. Three flight test manoeuvres at different flight altitudes. Subcritical, quasi-steady data points (1 drag count = 0.0001).

$C_{X_{w_o}}$	C_{GT}	$C_{MF}(10)$	$\Delta C_{MF}(20)$	$\Delta C_{MF}(30)$	$C_{X_{wC_L}}$	$C_{X_{wC_L^2}}$	
+1.000	+0.989	-0.998	-0.998	-0.998	+0.328	+0.485	$C_{X_{w_o}}$
	+1.000	-0.993	-0.993	-0.991	+0.360	+0.485	C_{GT}
		+1.000	+0.999	+0.999	-0.310	-0.457	$C_{MF}(10)$
			+1.000	+0.999	-0.305	-0.454	$\Delta C_{MF}(20)$
				+1.000	-0.298	-0.455	$\Delta C_{MF}(30)$
					+1.000	+0.863	$C_{X_{wC_L}}$
						+1.000	$C_{X_{wC_L^2}}$

Table 3. Correlation coefficients of parameter estimation errors resulting from a regression analysis with model 2 of C_{X_w} (Ref. Table 2).

$C_{X_{w_o}}$	C_{GT}		$\Delta C_{MF}(20)$	$\Delta C_{MF}(30)$	$C_{X_{w_{C_L}}}$	$C_{X_{w_{C_L^2}}}$	
+1.000	-0.555	-	-0.087	-0.288	+0.388	+0.670	$C_{X_{w_o}}$
	+1.000	-	+0.248	+0.692	+0.488	+0.032	C_{GT}
		-	-	-	-	-	
			+1.000	+0.565	+0.369	+0.214	$\Delta C_{MF}(20)$
				+1.000	+0.525	+0.111	$\Delta C_{MF}(30)$
					+1.000	+0.854	$C_{X_{w_{C_L}}}$
						+1.000	$C_{X_{w_{C_L^2}}}$

Table 4. Correlation coefficients of parameter estimation errors resulting from a regression analysis with model 1 of C_{X_w} (Ref. Table 2).

$C_{X_{w_o}}$	24
C_{GT}	10
$C_{MF}(10)$	64
$\Delta C_{MF}(20)$	73
$\Delta C_{MF}(30)$	46
$C_{X_{w_{C_L}}}$	1
$C_{X_{w_{C_L^2}}}$	1

Table 5. Comparison of estimation accuracies of model 2 with model 1 expressed as the ratio of normalized parameter estimation error standard deviations (Ref. Table 2).

	flight altitude (ft)	
$\bar{e}$	10.000 20.000 30.000	-0.0031 +0.0074 -0.0029
σ_e	10.000 20.000 30.000	0.0036 0.0045 0.0019
R_t		0.997855

Table 6. Total correlation coefficient and residuals of regression analysis with model of C_L. Three flight test manoeuvres at different flight altitudes. Subcritical, quasi-steady data points.

C_{L_o}	C_{L_α}	$C_{L_{\alpha M}}$	$C_{L_{\alpha M^2}}$	
+1.000	-0.283	+0.282	-0.322	C_{L_o}
	+1.000	-0.995	+0.981	C_{L_α}
		+1.000	-0.995	$C_{L_{\alpha M}}$
			+1.000	$C_{L_{\alpha M^2}}$

Table 7. Correlation coefficients of parameter estimation errors resulting from a regression analysis with model of C_L (Ref. Table 5).

	T_{CG}^*	Q^*
$\bar{e}$	-0.11 +0.51 -0.40	-0.0014 +0.0072 -0.0059
σ_e	16 11 22	0.021 0.019 0.045
R_t	0.999817	0.999159

Table 8. Total correlation coefficient and residuals of regression analysis with model of "dimensionless" thrust T_{CG}^* and "dimensionless" mass flow Q^*. Three flight test manoeuvres at different flight altitudes.

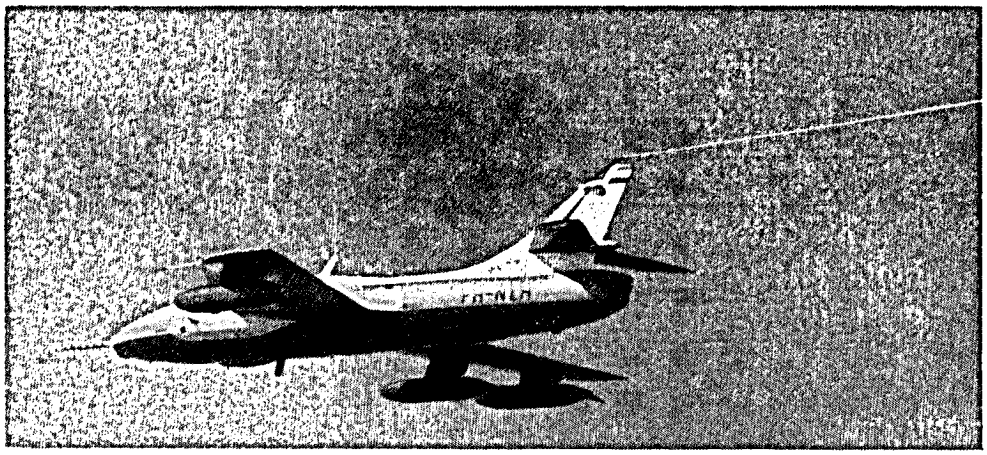

Fig. 1. Hawker Hunter laboratory aircraft with static pressure trailing cone.

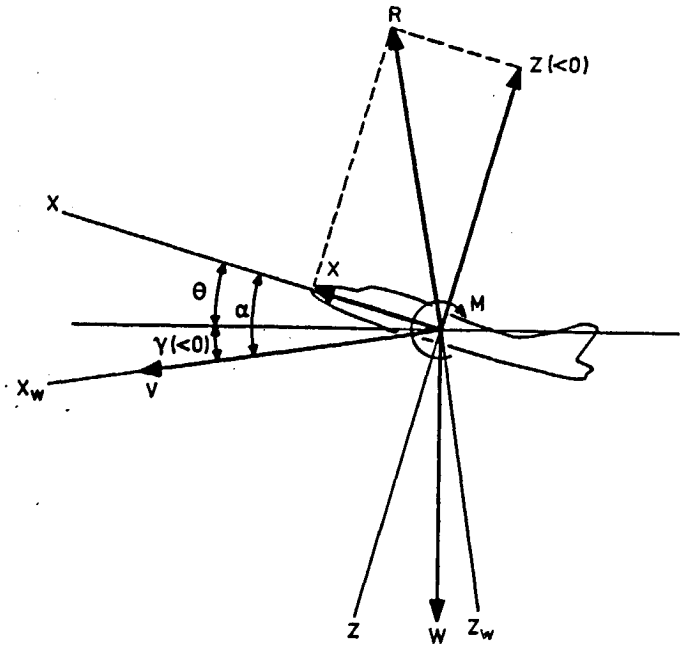

Fig. 2. Body and wind axes in symmetrical flight.

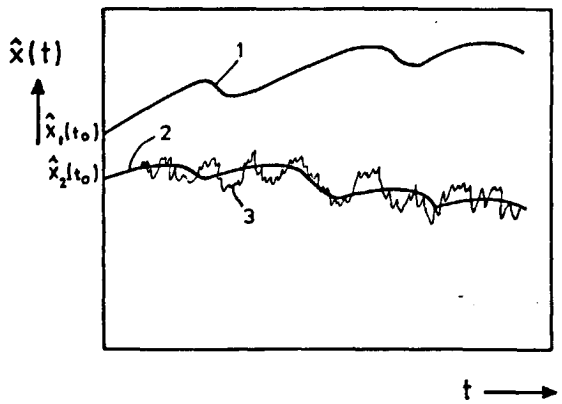

Fig. 3. Principle of aircraft trajectory estimation. Trajectory 1 from intertial information and initial State vector $\hat{x}_1$ (t_o), trajectory 2 from inertial information and "optimal" initial State vector $\hat{x}_2(t_o)$, resulting in a "best" fit to trajectory 3 from barometric measurements.

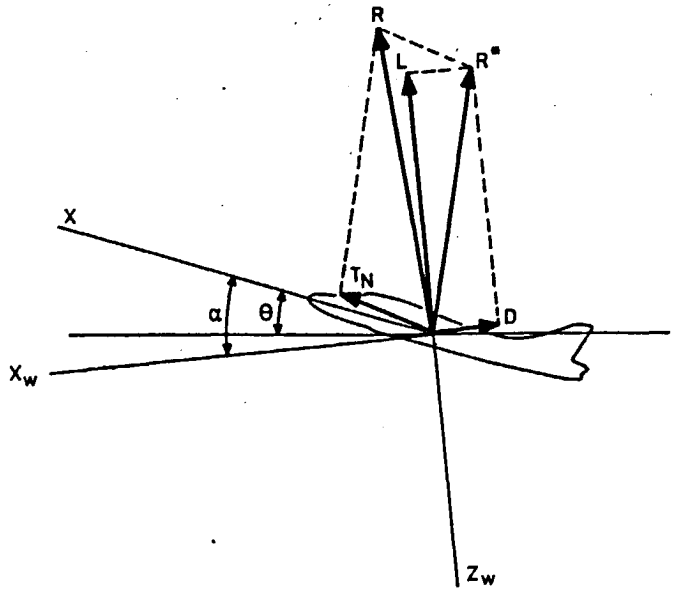

Fig. 4. Aerodynamic forces in symmetrical flight.

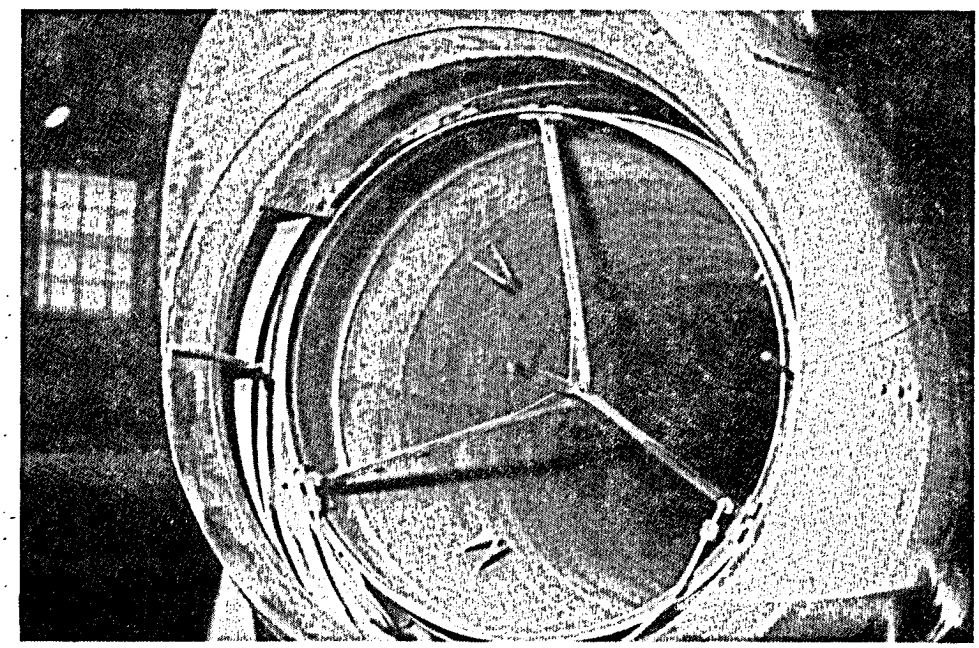

Fig. 5. Measurement of mean total pressure, central static pressure and total temperature in the jet pipe.

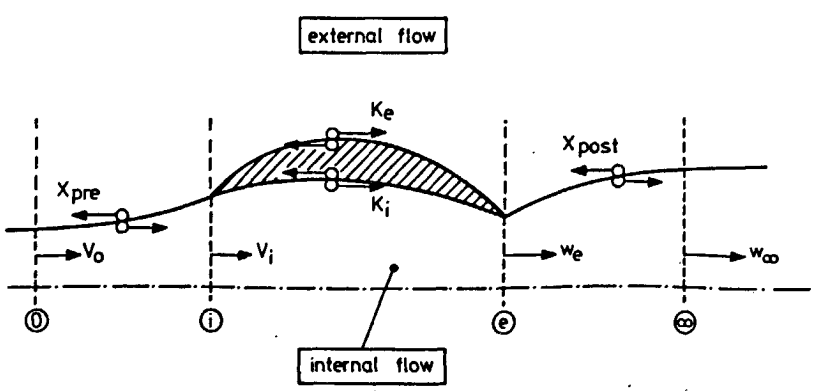

Fig. 6. Definition of engine net thrust.

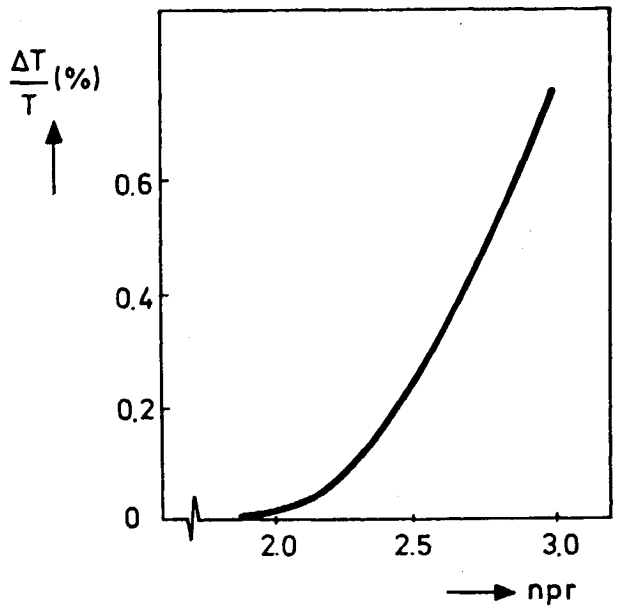

Fig. 7. Difference between Jones and Pearson net thrust.

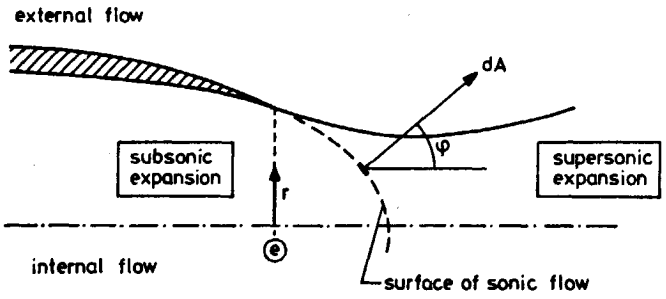

Fig. 8. Effect of Subsonic post exit expansion.

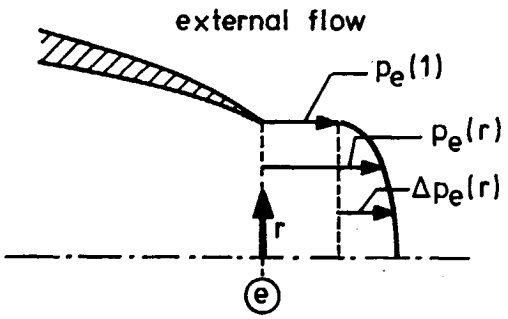

Fig. 9. Two-dimensional model for gross thrust and mass flow measurement.
$Pt_e(r)$ and $T_{te}(r)$ constant.
If npr > 1.85 then $p_e(1) > p_\infty$.
$\Delta p_e(r)$ is ellipsoid.

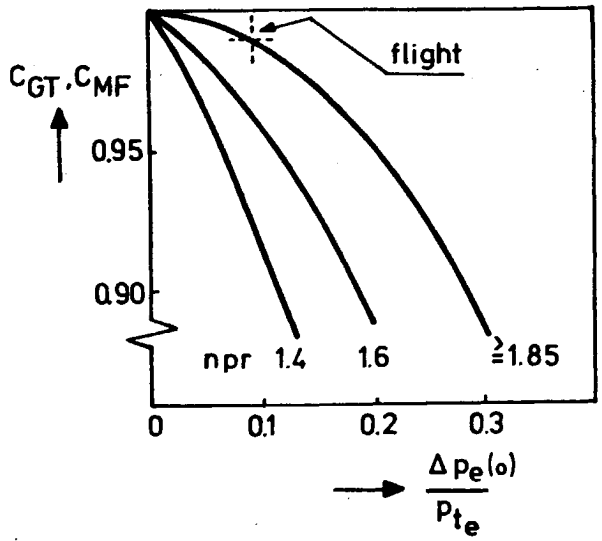

Fig. 10. Calulated gross thrust and mass flow calibration factors.

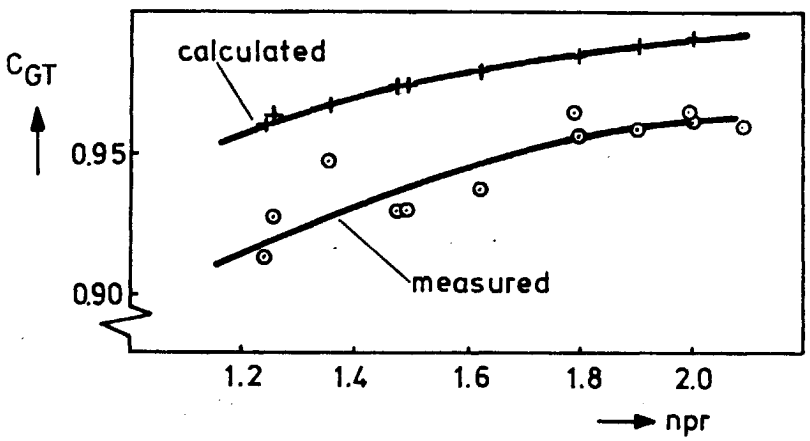

Fig. 11. Results static gross thrust calibration.

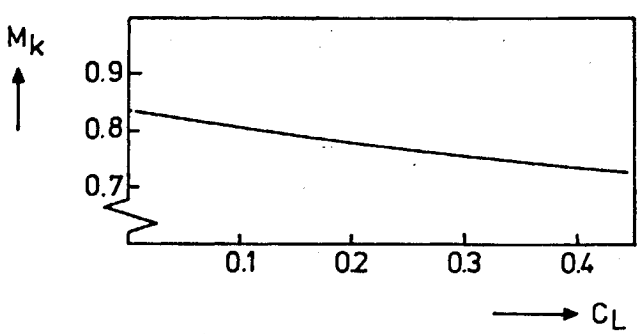

Fig. 12. Critical Mach number as a function of lift coefficient (Hoerner, Fluid dynamic Drag).

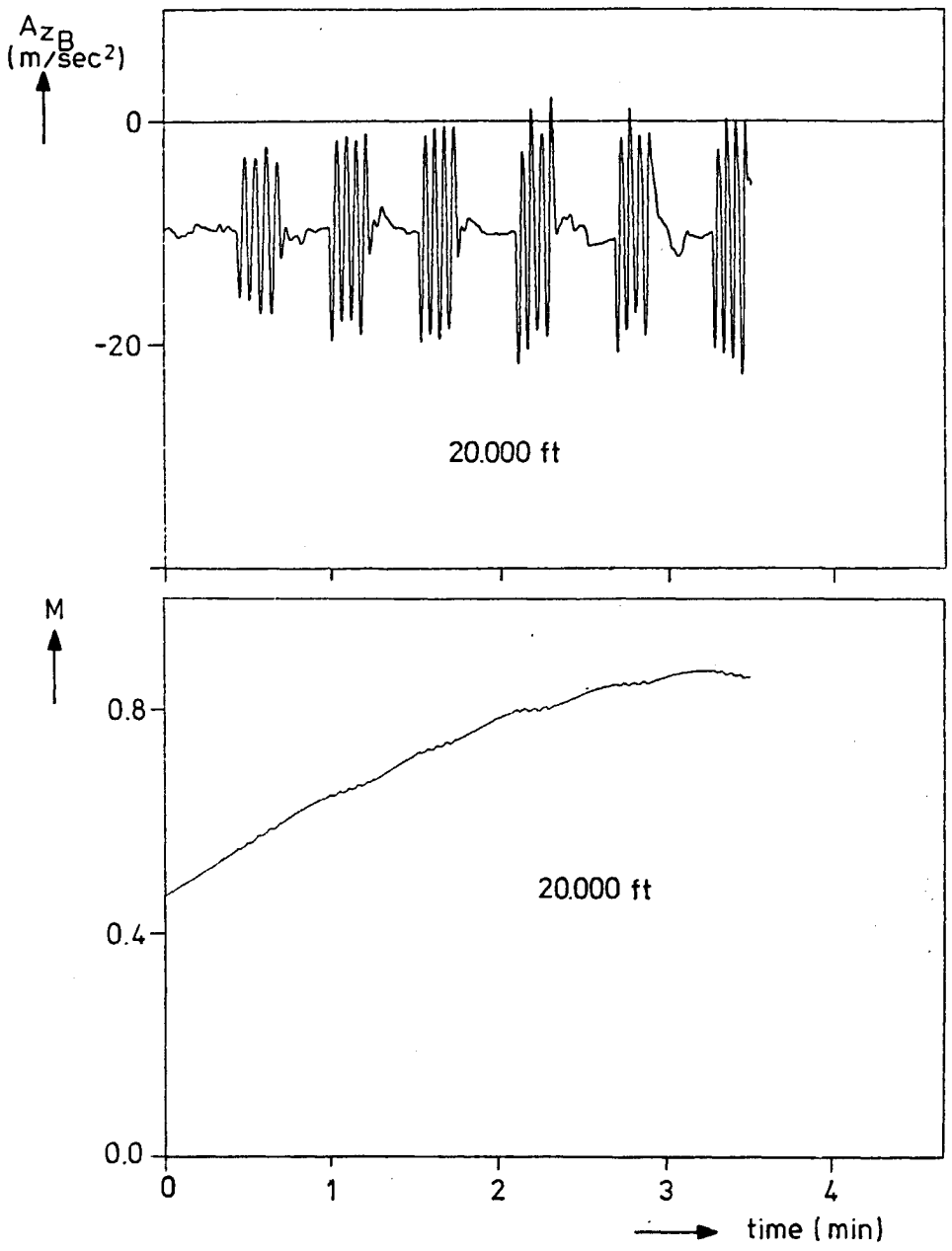

Fig. 13. Shape of non-steady flighttest manoeuvre.

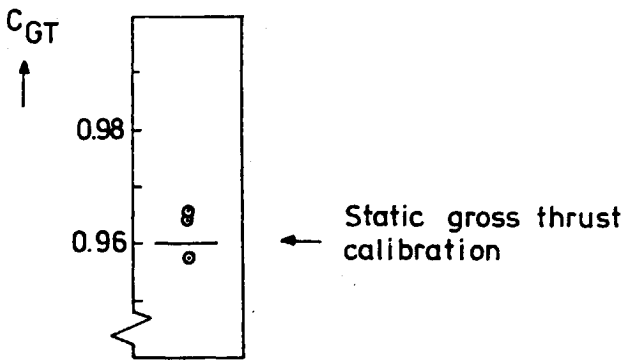

Fig. 14. Gross thrust calibration factor.
Each estimate obtained from 3 flighttest manoeuvres at different flight altitudes.

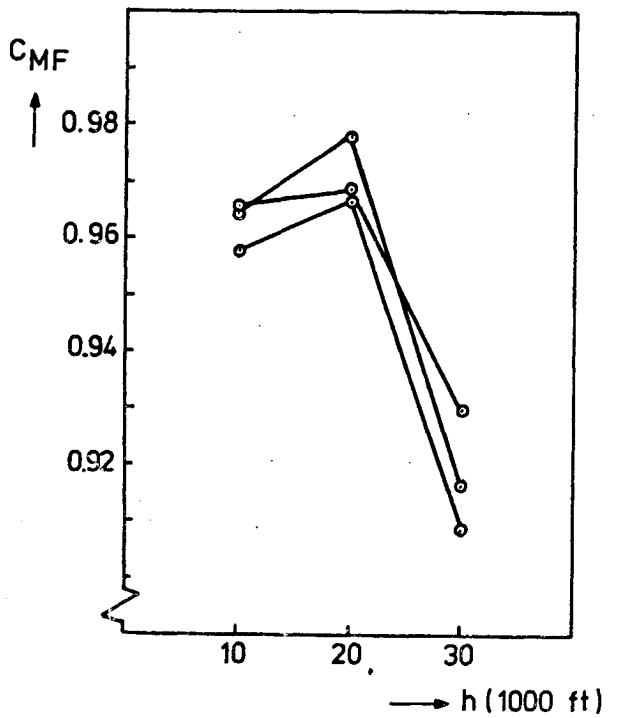

Fig. 15. Variation of mass flow calibration factor. Each estimate obtained from 3 flighttest manoeuvres at different flight altitudes.

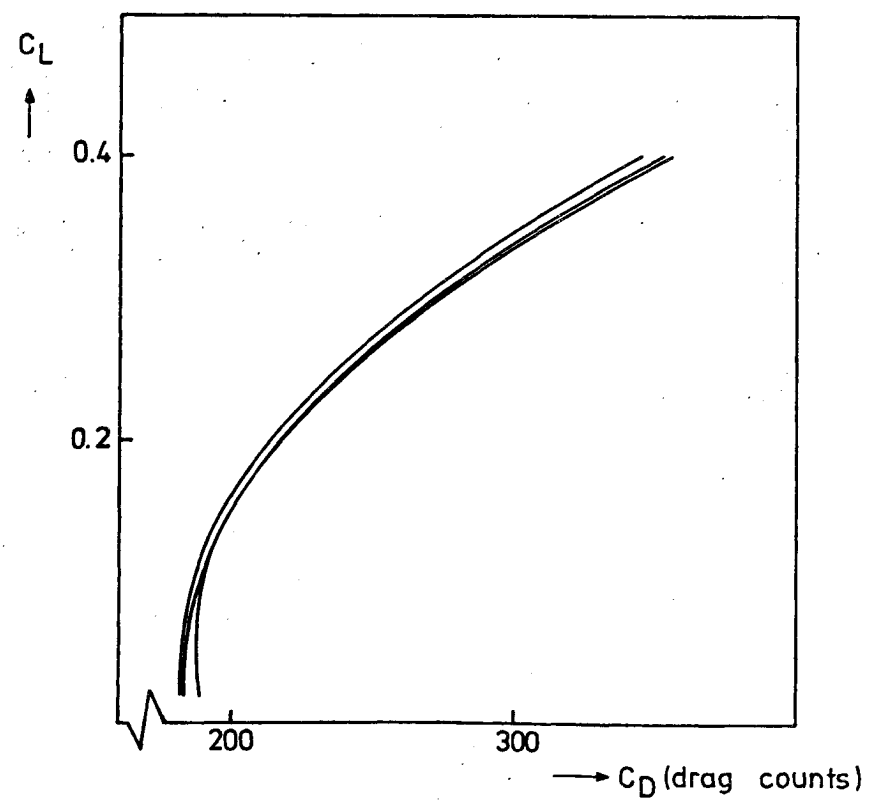

Fig. 16. Polar drag curves, no engine testbed data used. Each curve obtained from 3 flighttests manoeuvres at different flight altitudes.

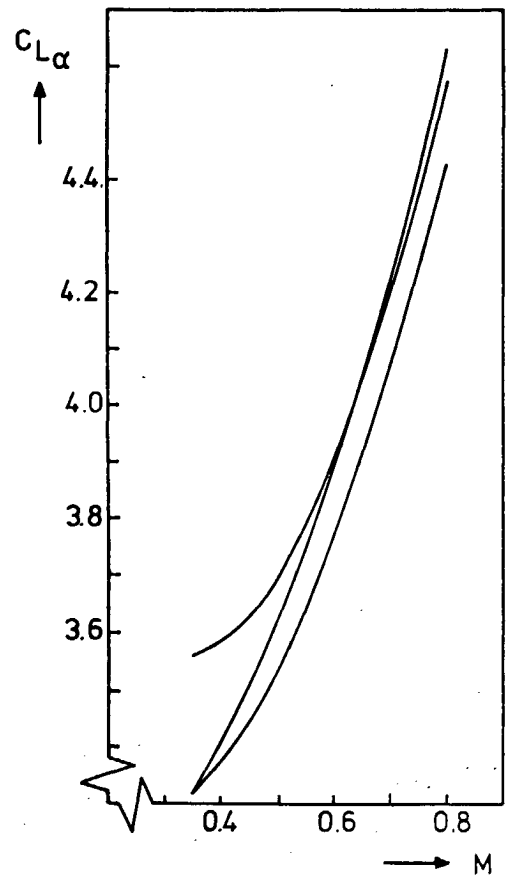

Fig. 17. C_{L_α} versus M curves. Each curve obtained from 3 flighttest manoeuvres at different flight altitudes.

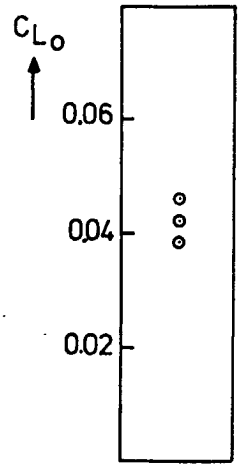

Fig. 18. Lift coefficient at zero angle of attack. Each estimate obtained from 3 flighttest manoeuvres at different flight altitudes.

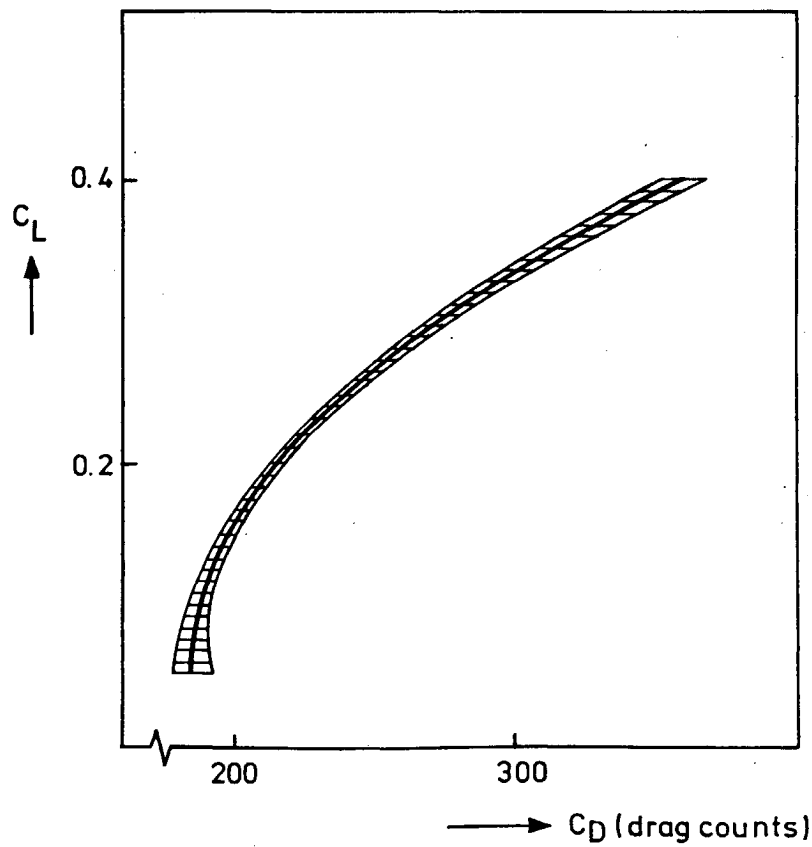

Fig. 19. Polar drag curve, mean and standard deviation obtained from 9 flighttest manoeuvres at different flight altitudes.
One set of values used for gross thrust and mass flow calibration factors.

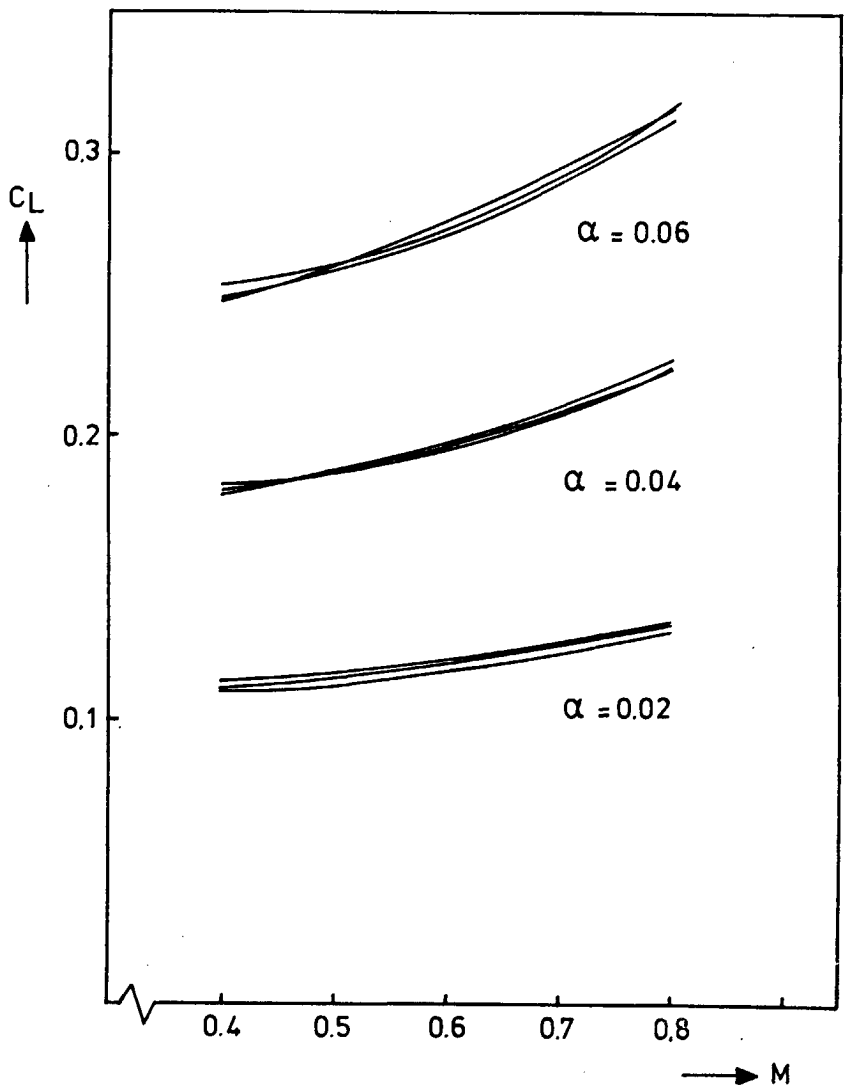

Fig. 20. Lift carpet. Each set of curves obtained from 3 flighttest manoeuvres at different flight altitudes.

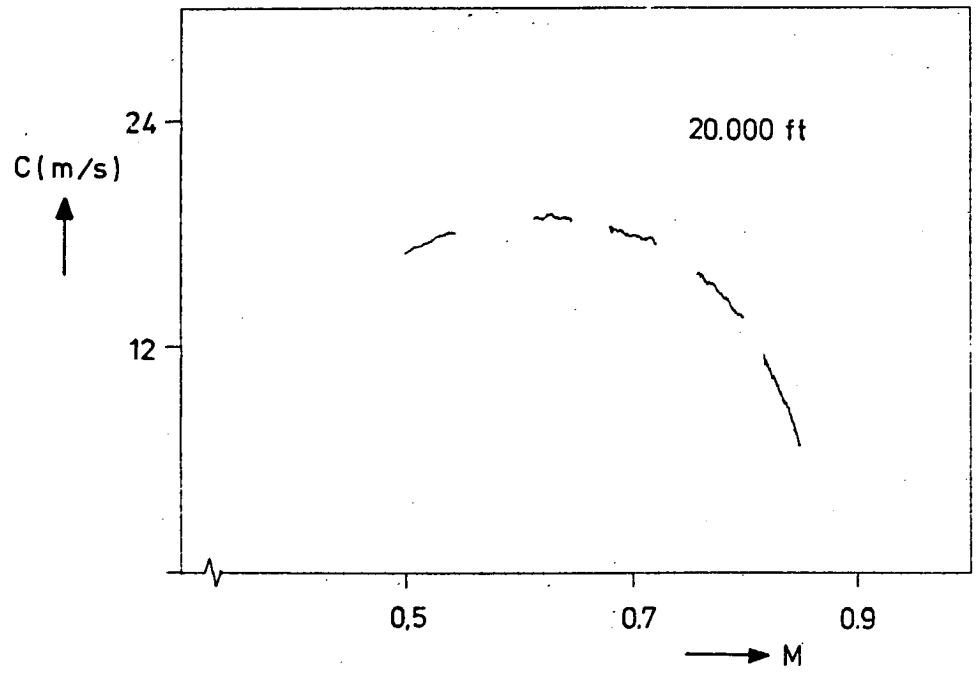

Fig. 21. Rate of climb versus Mach number in steady straight flight.

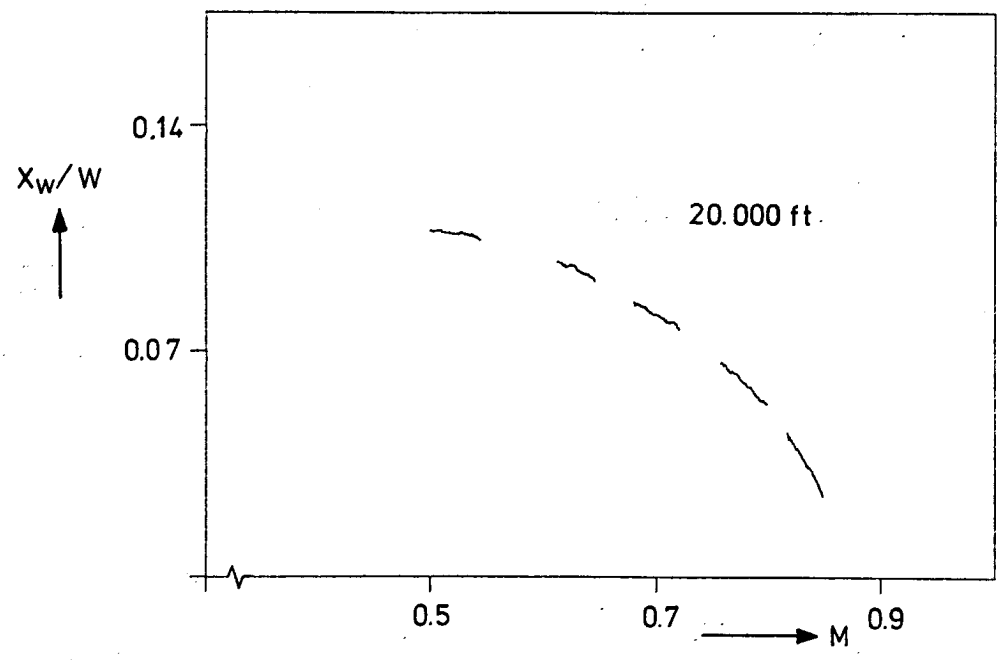

Fig. 22. Dimensionless excess thrust versus Mach number in horizontal accelerating flight.

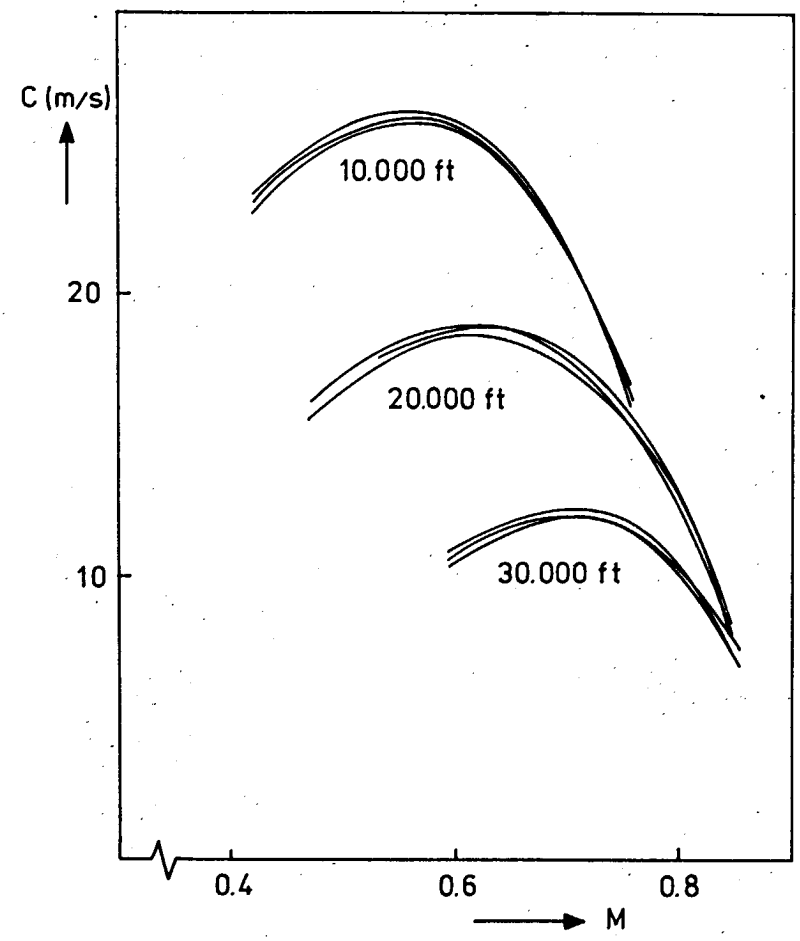

Fig. 23. Rate of climb versus Mach number curves, steady straight flight 9 flighttest manoeuvres.

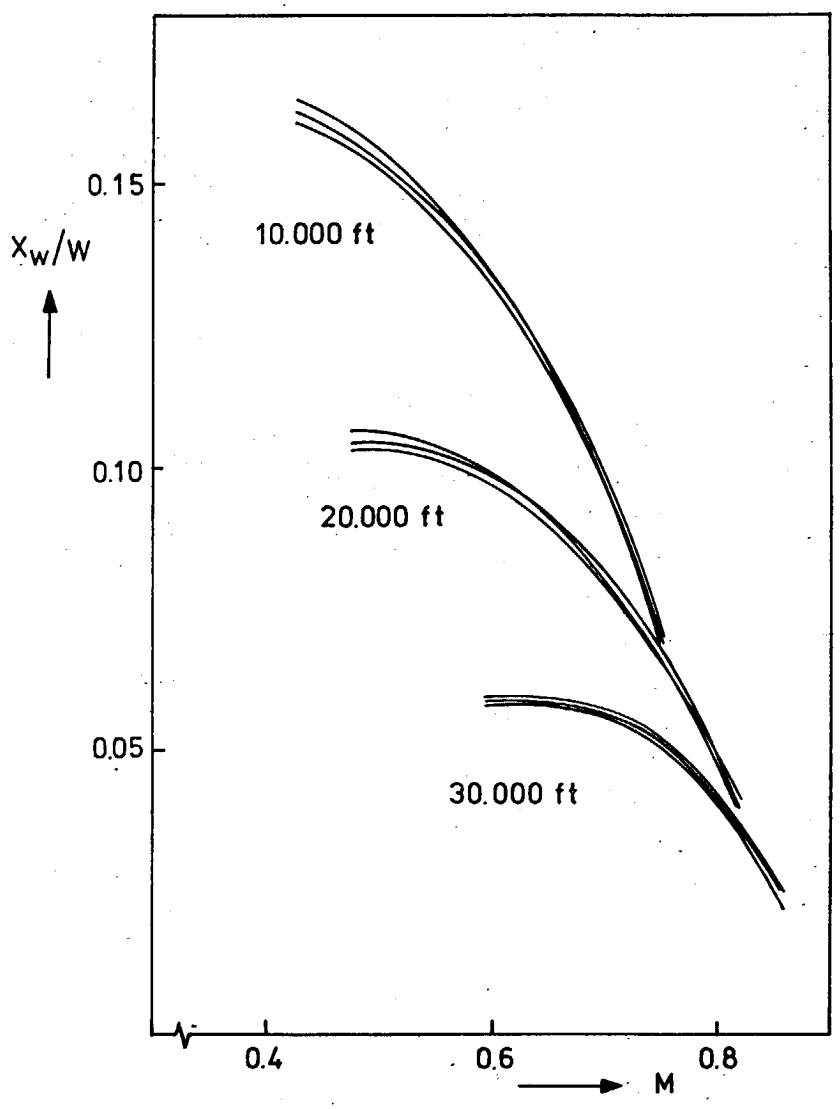

Fig. 24. Curves of dimensionless excess thrust versus Mach number, horizontal accelerating flight 9 flighttest manoeuvres.

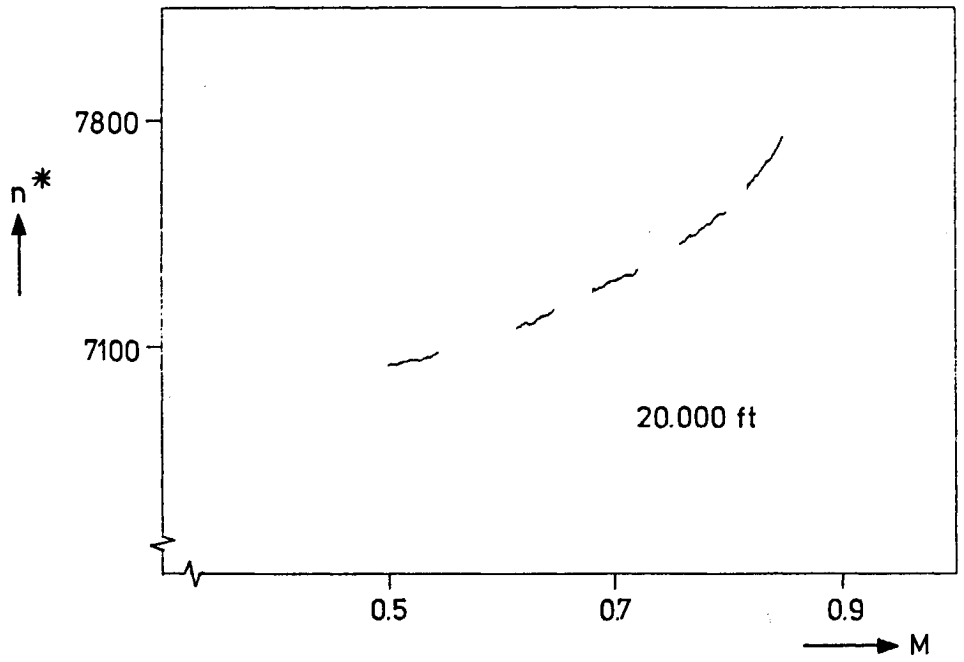

Fig. 25. Dimensionless engine rpm versus Mach number in steady horizontal flight.

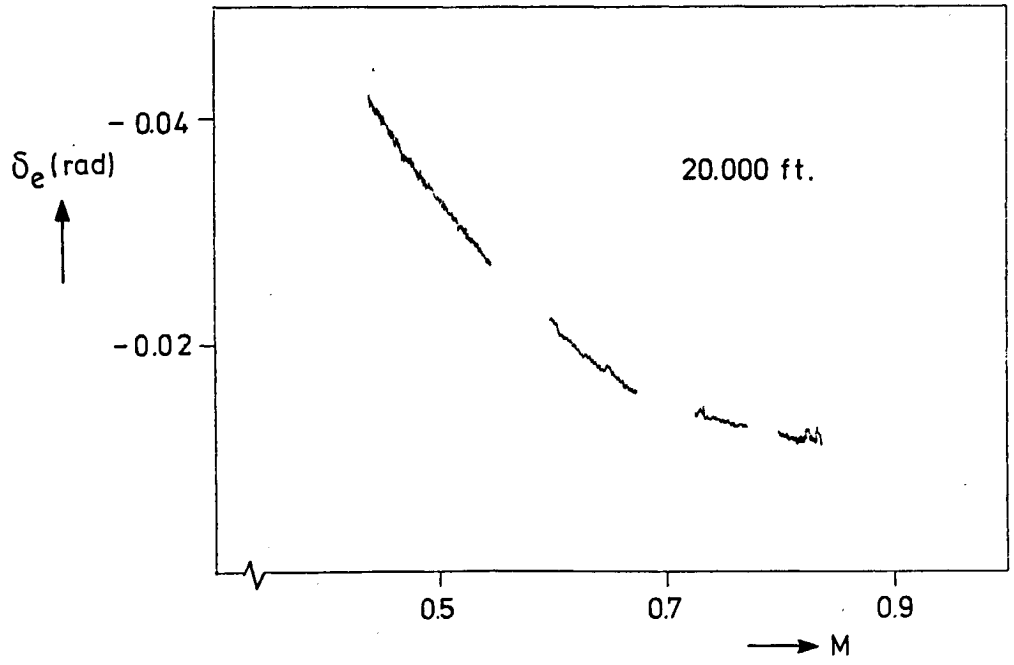

Fig. 26. Elevator angle versus Mach number in steady straight flight.

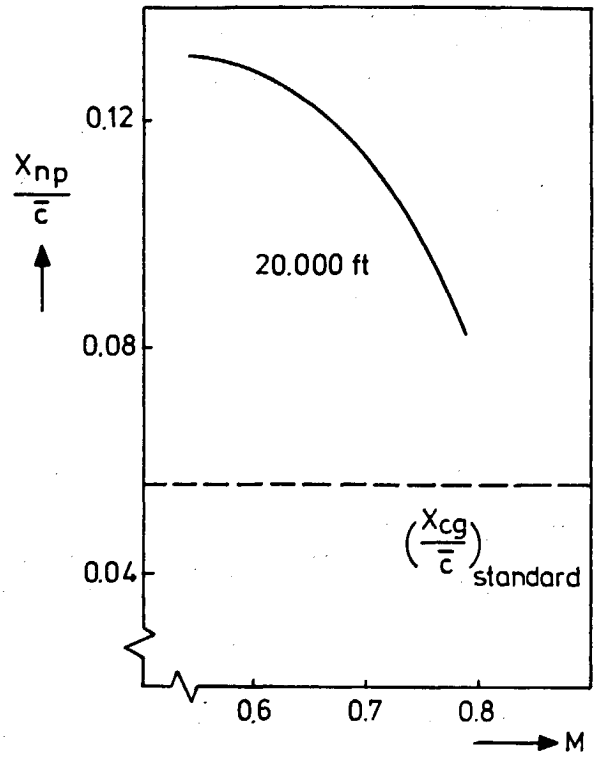

Fig. 27. Neutral point versus Mach number.
Steady straight flight.

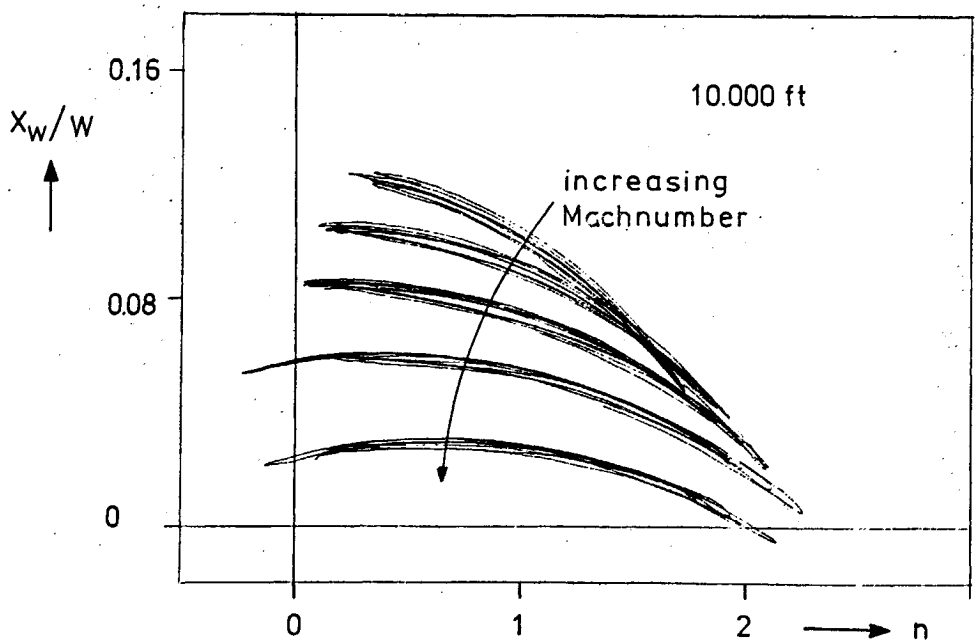

Fig. 28. Dimensionless excess thrust versus normal
load factor in horizontal manoeuvring flight.

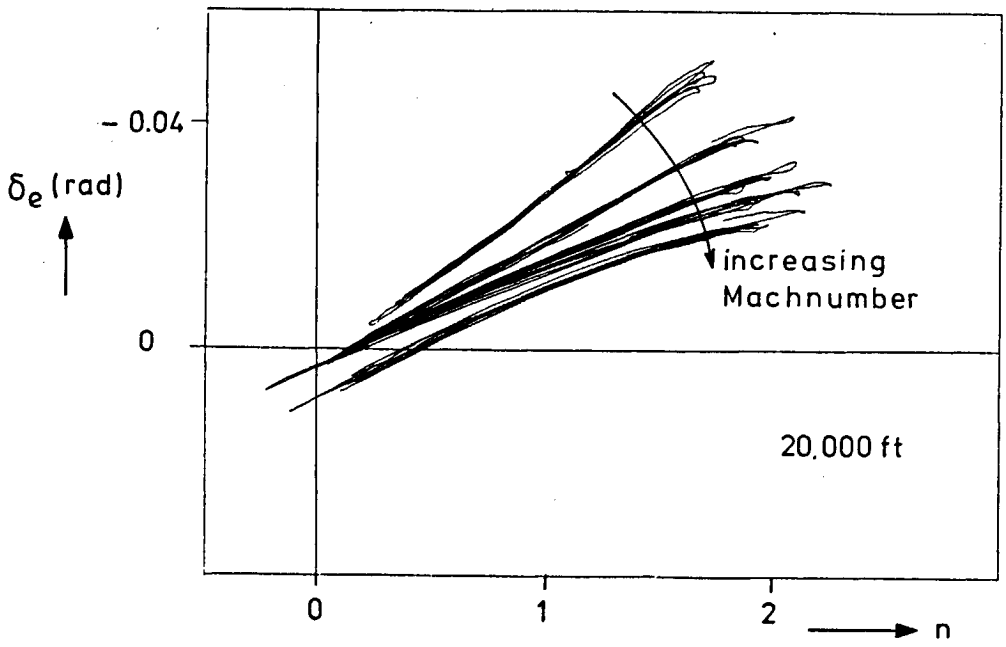

Fig. 29. Elevator angle versus normal load factor in horizontal manoeuvring flight.

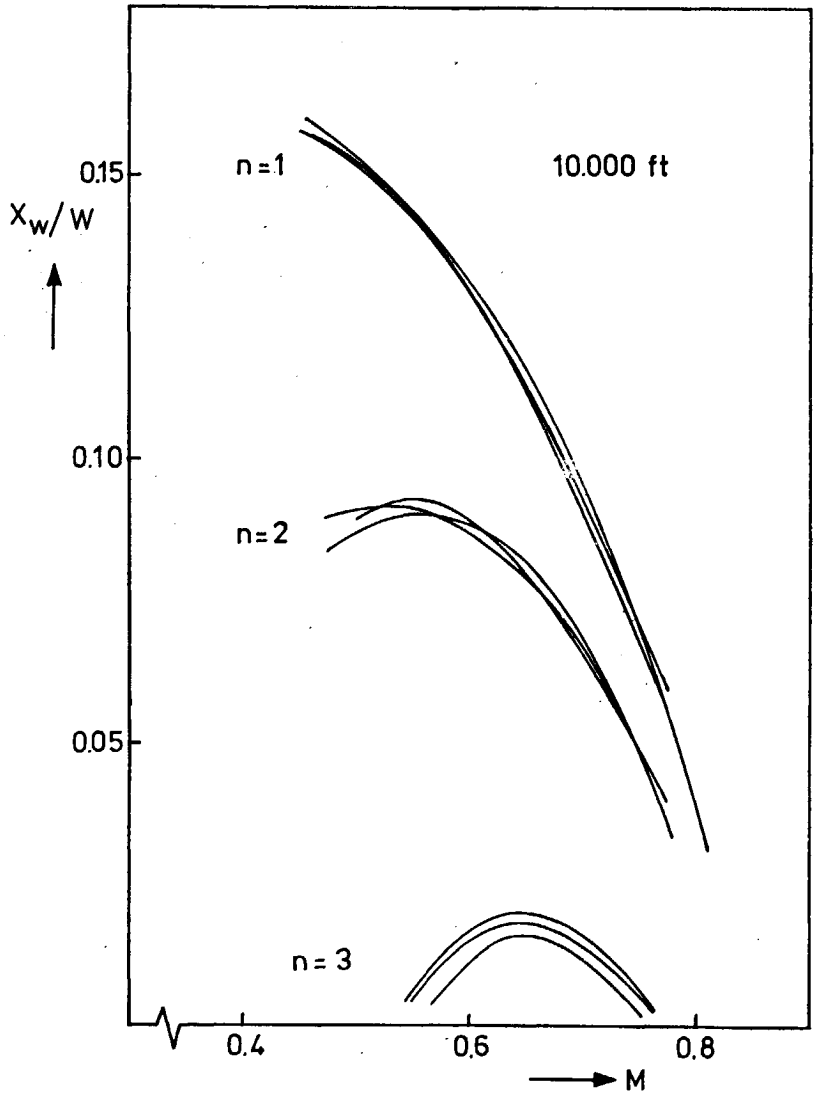

Fig. 30. Curves of dimensionless excess thrust versus Mach number, horizontal manoeuvering flight, 3 flight test manoeuvres.

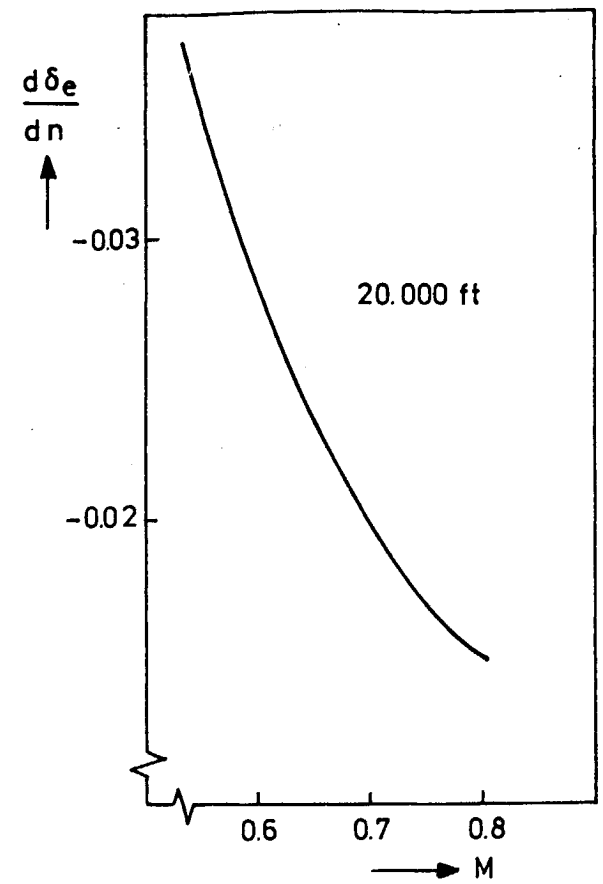

Fig. 31. Stick displacement per "g" versus Mach number horizontal manoeuvring flight.

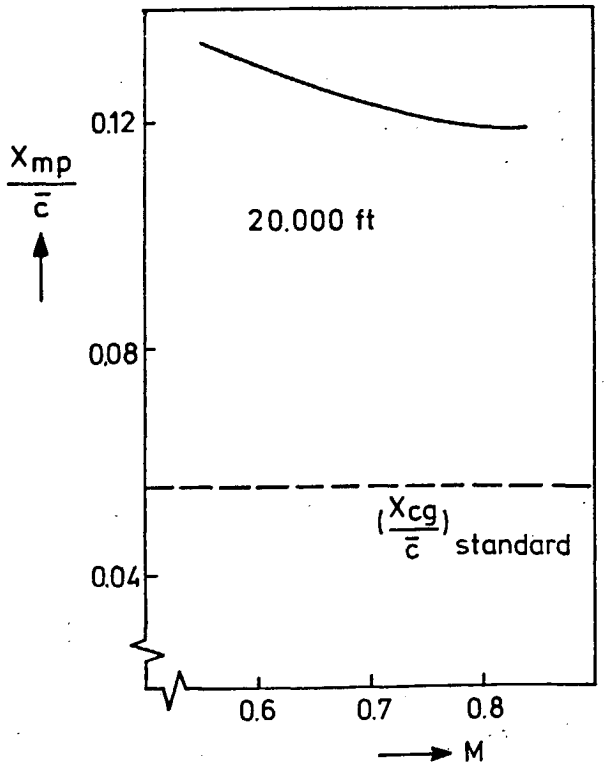

Fig. 32. Manoeuvre point versus Mach number horizontal manoeuvring flight.